Investigation on Liquid Flow Characteristics in Microtubes

Qiao-Li Chen, Ke-Jun Wu, and Chao-Hong He
Dept. of Chemical and Biological Engineering, State Key Laboratory of Chemical Engineering, Zhejiang University, Hangzhou 310027, China

DOI 10.1002/aic.14656
Published online November 3, 2014 in Wiley Online Library (wileyonlinelibrary.com)

The fundamental understanding and prediction of liquid flow characteristics in microscale are important to control the performance of microfluidic devices. However, fundamental questions about liquid flow characteristics in microscale have not been settled yet and systematical investigation is needed. A systematical investigation on liquid flow characteristics through microtubes with diameters varying from 44.5–1011 μm and relative roughness in the range 0.02–4.32% in the Reynolds number range 29–11,644 was performed in this work, using water as working fluid. Experimental results indicated that early transition occurred when the diameter was smaller than 1000 μm, the transitional flow characteristics for smooth microtubes differed from rough microtubes and the friction factor in turbulent region for rough microtubes was larger than conventional theory. Moreover, a parameter α was proposed to describe the characteristic of microtube. The characteristic parameter was used to calculate the critical Reynolds number and the friction factor in turbulent region for microscale. © 2014 American Institute of Chemical Engineers *AIChE J*, 61: 718–735, 2015
Keywords: microfluidic, microtube, liquid flow characteristics, critical Reynolds number, friction factor

Introduction

Microscale systems have attracted much attention of researchers[1–8] and are believed to play an important role in chemical processes. The fundamental understanding and prediction of the liquid flow characteristics such as velocity distribution and pressure loss in microscale are important to control the performance of microfluidic devices. Microscale is defined to be one with diameter or hydraulic diameter less than 1000 μm in literature[9–13] as well as in this work. A large number of experimental investigations with focus on liquid flow characteristics in microscale have been reported and a brief overview of these researches has been presented in the most recent reviews.[14–17] As can be found in these reviews, the liquid flow characteristics in microscale different researchers observed are inconsistent. Besides, among all the experimental studies,[14–17] studies of laminar flow characteristics are mostly addressed while studies of transitional and turbulent flow characteristics seem to be in a lack. The liquid flow characteristics for the whole flow regions in microscale are still unclear.

The flow characteristics were usually quantitatively analyzed based on the Reynolds number and friction factor in literature. To understand the liquid flow characteristics, there are four basic questions to be explored. (1) Whether the friction factor of laminar flow in microscale is still the same as conventional theory? Will it be affected by the decrease of diameter, increase of roughness or other factors? (2) Can early transition, which means early departure from laminar flow (lower critical Reynolds number than conventional theory), be observed in microscale? If the answer is yes, then what is the cause of early transition? (3) Is there any difference between the transitional flow characteristic in microscale and that in conventional scale? (4) Whether the friction factor of turbulent flow in microscale can be predicted by conventional theory.

There are about a hundred references related to microscale flows that have discussed question one. The most representative ones are listed in this paragraph. Peng et al.[18] and Jiang et al.[19] found that smaller channels had lower friction factor (in laminar flow region), while Mala and Li [20] reported that as the Reynolds number increased, a significant higher friction factor than that predicted by conventional theory was observed and the deviation increased as the microtube diameter decreased. Some other researchers[21–24] also observed higher friction factor (in laminar flow region). However, most recently, researchers[25–30] generally agreed that friction factor (in laminar flow region) fitted well with conventional theory within experimental uncertainties. The details about the references mentioned above are listed in Table 1.

A lot of references mentioned critical Reynolds number in their studies though not as much as those focused on laminar flow. However, fewer references gave specific values of critical Reynolds number according to different dimensions (such as diameters or roughnesses) of microtubes (or microchannels) and even limited number of references gave further discussion on critical Reynolds number. Some researchers[31–34] found that the critical Reynolds number was around 1800–2000 and considered that the same as conventional theory. However, most researchers[18,22,23,35–43] thought that early transition exists. Broadly speaking, there are two views on the cause of early transition. One view is that the

Additional Supporting Information may be found in the online version of this article

Correspondence concerning this article should be addressed to: K.-J. Wu at: wkj@zju.edu.cn.

Table 1. Details About Literature on Liquid Flow Friction Factor (of Laminar Flow) in Microscale

Reference	Material	Geometry	Test fluids	D_h (μm)	$\varepsilon \cdot D_h^{-1}$ (%)	Re	$(fRe)_{exp} \cdot (fRe)_{the}^{-1}$ (laminar flow)	Uncertainty in f (%)
Peng et al.[18]	SS	Rectangle	Water	133–343	0.6–1	50–4000	<1	10
Jiang et al.[19]	Silicon	Trapezoid	Water	35–120	<0.4	1–30	<1	–
Mala et al.[20]	SS,FS	Circular	Water	50–254	0.7–3.5	100–2000	>1	9.2
Stanley et al.[21]	Aluminum	Rectangle	Water	56–256	0–0.16	50–10000	>1	–
Pfund et al.[22]	Polymide	Rectangle	Water	253–1900	Smooth	60–3450	>1	5.4–11.1 (uncertainty n fRe)
Li et al.[23]	SS	Circular	Water	128.76–179.8	3–4	350–2500	>1	<10 (uncertainty in fRe)
Ergu et al.[24]	Acrylic	Rectangle	Water	208	Smooth	100–845	>1	18.77
Hao et al.[25]	Silicon	Trapezoid	Water	237	0.025	50–2800	≈1	–
Hrnjak and Tu[26]	PVC	Rectangle	R134a	69.5–304.7	0.14–0.35	112–9180	≈1	6.2
Park and Punch[27]	Silicon	Rectangle	Water	106–307	Smooth	69–800	≈1	9.2
Schilder et al.[28]	Glass	Circular	Water	600	Smooth	20–1200	≈1	–
Aniskin et al.[29]	Glass	Circular	Water	24.5–34.5	Smooth	13–330	≈1	–
Barlak et al.[30]	SS	Circular	Water	200–589	–	75–10461	≈1	12.92–19.76

SS and FS stand for stainless steel and fused silica, respectively.

decrease of diameter leads to an occurrence of early transition. Peng et al.[18] found that the laminar flow transition occurred at Reynolds number in the range of 200–700 and the critical Reynolds number was strongly affected by the hydraulic diameter. Pfund et al.[22] also found that the critical Reynolds number decreased further with decreasing channel depth. However, the critical Reynolds number values they observed were much larger than the values of 200–700. In some other studies,[39,43] they listed the specific values of critical Reynolds number of each microtube and proposed the same conclusion as Peng et al.[18] and Pfund et al.[22] that the smaller the microtube diameter, the lower the critical Reynolds number. The other view is that the increase of roughness leads to lower critical Reynolds number in microscale. Tang et al.[40] observed that the transition from laminar to turbulent flow occurred earlier and attributed the result to surface roughness effect. Kandlikar et al.[41] also suggested that the laminar to turbulent transition was seen to occur at lower Reynolds number with an increase in the roughness. In their later work,[42] they did more experiments to support their conclusion. The details about the references mentioned above are listed in Table 2.

Only a few reports discussed the liquid flow characteristic in the transitional flow region. Almost all the related references are listed in this paragraph. Some researchers[33,35,44–47] thought that the transitional flow region in microscale could be regarded as the same as conventional theory though the specific Reynolds number ranges of transition flow they observed were different. Some researchers observed different transitional flow characteristics in microscale as compared with conventional scale and thought that it was caused by the effect of roughness. Bucci et al.[48] found that the smallest microtube (diameter 172 μm) with the highest value of relative roughness (0.87%) showed a "rough" laminar to turbulent flow transition while the other two microtubes showed a "smooth" laminar to turbulent flow transition ("rough" meant that the friction factor in the transitional region increased quickly as the Reynolds number increased and "smooth" meant that the friction factor in the transitional region increased slowly as the Reynolds number increased). They attributed this effect to the increase of surface roughness. Barlak et al.[30] noticed "smooth" and "rough" transition for different microtubes, too. Some other researchers observed different transtional flow characteristics in microscale, but

Table 2. Details About Literature on Liquid Flow Critical Reynolds Number in Microscale

Reference	Material	Geometry	Test fluids	D_h (μm)	$\varepsilon \cdot D_h^{-1}$ (%)	Re	Early Re_c	Uncertainty in f (%)
Agostini et al.[31]	Aluminum	Rectangle	R-134a	770–1170	–	500–6500	No	7–15
Rands et al.[32]	FS	Circular	Water	16.6–32.2	0.03–0.04	300–3400	No	16–29 (uncertainty in fRe)
Yang and Lin[33]	SS	Circular	Water	123–962	0.15–1.14	150–10000	No	0.2–5.3
Dutkowski[34]	SS	Circular	Water	550–1100	–	30–6500	No	–
Li et al.[23]	SS	Circular	Water	128.76	3–4	350–2500	Yes	<10 (uncertainty in fRe)
Hao et al.[35]	Glass	Circular	Water	230	0.74	1540–2960	Yes	–
Xu et al.[36]	Silicon	Rectangle	Water	30–344	<1	20–4000	Yes	<12
Sharp and Adrian[37]	Glass	Circular	Water	50–247	–	20–2900	Yes	–
Liu et al.[38]	SS	Circular	Water	168–399	2.7–3.5	100–3000	Yes	7.5
Peng et al.[18]	SS	Rectangle	Water	133–343	0.6–1	50–4000	Yes	10
Pfund et al.[22]	Polymide	Rectangle	Water	253–1900	Smooth	60–3450	Yes	5.4–11.1 (uncertainty in fRe)
Zhao and Liu[39]	SS,FS	Circular	Water	168–799	0–8	50–2700	Yes	6.5
Tang et al.[40]	SS	Circular	Water	119–172	4.1–5.9	10.5–1100	Yes	6.3
Kandlikar et al.[41]	–	Rectangle	Water	325–1819	0–14	200–5700	Yes	8.81
Brackbill and Kandlikar[42]	–	Rectangle	Water	198–1084	0–5.18	30–7000	Yes	7.58
Ghajar et al.[43]	SS	Circular	Water	337–2083	1–4	500–7000	Yes	–

SS and FS stand for stainless steel and fused silica, respectively.

Table 3. Details About Literature on Liquid Flow Characteristics (of Transitional Flow) in Microscale

Reference	Material	Geometry	Test fluids	D_h (μm)	$\varepsilon \cdot D_h^{-1}$ (%)	Re	Transitional Flow Characteristics	Uncertainty in f (%)
Hegab et al.[44]	Aluminum	Rectangle	R-134a	112–210	0.16–0.89	1280–13000	Re_t 4000	3–23
Celata et al.[45]	SS	Circular	R114	130	2.65	100–8000	Re_t 2480	6–9
Yang and Lin[33]	SS	Circular	Water	123–962	0.15–1.14	150–10000	Re_t 3000	0.2–5.3
Hao et al.[35]	Glass	Circular	Water	230	0.74	1540–2960	Re_t 2500	–
Vijayalakshmi et al.[46]	Silicon	Trapezoid	Water	60.5–211	0.04–0.18	320–2791	Re_t 3500	0.12–5.34
Elsnab et al.[47]	Aluminum	Rectangle	Water	923	0.06	173–4830	Re_t 2700	–
Bucci et al.[48]	SS	Circular	Water	172	0.87	100–3600	rough transition	8.36
Yang et al.[49]	–	Circular	Water, R-134a	502–4010	–	110–40000	increases with decreasing tube diameters	4.1–9.0
Ghajar et al.[43]	SS	Circular	Water	337–667	1–4	500–7000	narrower	–
Barlak et al.[30]	SS	Circular	Water	200–589	–	75–10461	smooth and rough transition	12.92–19.76

SS stands for stainless steel.

thought that it was due to the decrease of diameter. Yang et al.[49] found that the transition Reynolds number varied from 1200 to 3800 and increased with decreasing microtube diameter. Ghajar et al.[43] held the opinion that the Reynolds number range for transition flow became narrower with the decrease in microtube diameter. Moreover, Ghajar et al.[43] observed that further decrease in the microtube diameter from 667 to 337 μm caused the transition Reynolds number shifting from 3000 to 1700, which was lower than conventional theory. The details about the references mentioned above are listed in Table 3.

With respect to question four, the number of related references is also limited. Almost all the related references are listed in this paragraph. Large diversities exist between different references. Hegab et al.[44] observed that the friction factor was lower than that predicted by commonly used conventional scale correlations[50] for flows in the turbulent region. Bucci et al.[48] and some other researchers[33,49] found that the friction factor (in turbulent flow region) agreed well with conventional scale correlations.[51,52] However, Celata et al.[45] found that the friction factor (in turbulent flow region) was higher than that predicted by Blasius equation[52] but lower than that by the Colebrook equation[51] with the experimental value of relative roughness. Agostini et al.[31] also found that the friction factor (in turbulent flow region) was higher than that predicted by Blasius equation.[52] Kandlikar et al.[41] found that the friction factor (in turbulent flow region) was considerably above the constant value obtained according to Miller equation.[53] Hrnjak and Tu[26] found that the friction factor (in turbulent flow region) followed Churchill's equation[54] with $\varepsilon \cdot D_h^{-1}$ of about 0.7, 0.5, 2.0, and 0.3% for test section with $\varepsilon \cdot D_h^{-1}$ of 0.16, 0.14, 0.35, and 0.29%, respectively. The details about the references mentioned above are listed in Table 4.

To sum up, these basic questions have not been settled yet and systematical investigation is needed. While not attempting to answer these questions with surprising new findings, we tried to review the experimental results in literature, eliminate some confusion by carefully identifying and controlling experimental methods, systematically and quantitatively answer these questions based on the experimental data in this work and literature. Circular microtubes were used in this work and deionized degassed water was used as working fluid. Experiments were carried out to study the laminar, transitional, and turbulent flow characteristics of water in 20 different microtubes with Reynolds number ranging from 29–11,644, especially focused on the critical Reynolds number and friction factor in turbulent flow. Flow characteristics in three types namely 316 stainless steel (SS), poly-ether-ether-ketone (PEEK), and fused silica (FS) of microtubes with their diameters ranging from 44.5–1011 μm and roughness (relative roughness) varying from 0.1–5.2 μm (0.02–4.32%) have been studied. The major objectives of this work are to conduct accurate measurements in test section and answer the four basic questions, especially the questions about critical Reynolds number and friction factor in turbulent flow region, quantitatively.

Experimental Setup

Experimental apparatus

The experimental apparatus was designed to be accurate and versatile, which accommodated the use of multiple diameters and lengths of tested microtubes. The apparatus

Table 4. Details About Literature on Liquid Flow Friction Factor (of Turbulent Flow) in Microscale

Reference	Material	Geometry	Test fluids	D_h (μm)	$\varepsilon \cdot D_h^{-1}$ (%)	Re	f (turbulent flow)	Uncertainty in f (%)
Hegab et al.[44]	Aluminum	Rectangle	R-134a	112–210	0.16–0.89	1280–13000	< Bhati and Shah equation[50]	3–23
Bucci et al.[48]	SS	Circular	Water	290–520	0.31–0.75	100–6000	≈Colebrook correlation[51]	8.36
Yang et al.[49]	–	Circular	Water, R-134a	502–4010	–	110–40000	≈Blasius equation[52]	4.1–9.0
Yang and Lin[33]	SS	Circular	Water	123–962	0.15–1.14	150–10000	≈Blasius equation[52]	0.2–5.3
Celata et al.[45]	SS	Circular	R114	130	2.65	100–8000	Colebrook equation[51]>f> Blasius equation[52]	6–9
Agostini et al.[31]	Aluminum	Rectangle	R–134a	770–1170	–	500–6500	>Blasius equation[52]	7–15
Kandlikar et al.[41]	–	Rectangle	Water	684–953	7.35–11.08	200–3000	>Miller equation[53]	8.81
Hrnjak and Tu[26]	PVC	Rectangle	R-134a	104.1–304.7	0.14–0.35	112–9180	> Churchill equation[54]	4.5–6.3

SS stands for stainless steel.

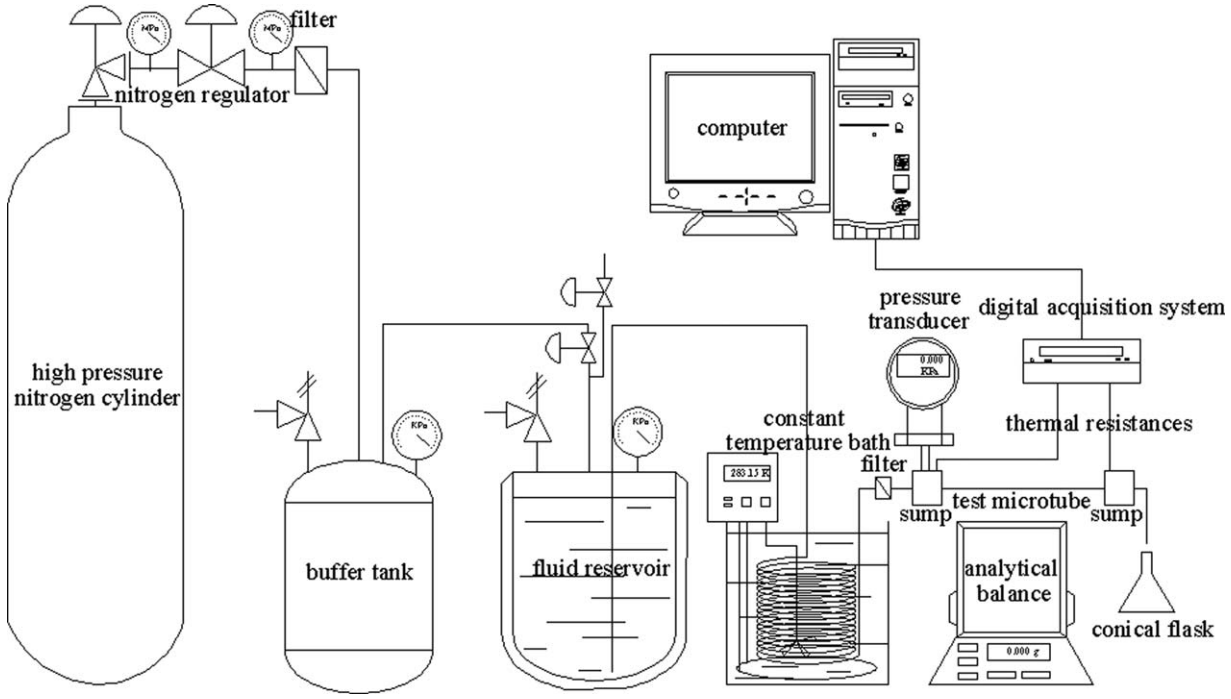

Figure 1. Schematic diagram of the experimental setup.

consists of two major components, including pressure system and test section. The overall schematic for the apparatus is presented in Figure 1.

The pressure system is comprised of a high pressure nitrogen cylinder (Jingong Air Co.), a 316 SS buffer tank (maximum working pressure 6.4 MPa, volume 3 L), a 316 SS fluid reservoir (maximum working pressure 6.4 MPa, volume 9 L) and a constant temperature bath (Shanghai Rongfeng 501A). The liquid is pressurized either by a compressed, inert gas or a pump in literature.[55] The high pressure nitrogen cylinder is chosen as the pressure source in this work as it is a stable pressure source, indissolvable in water, and preferred by researchers.[24,29,30,33,35,40,43,46,56–58] The high purity nitrogen in the high pressure cylinder is pressurized to approximate 17 MPa by the distributor. Two precise nitrogen regulators are used to control the pressure of nitrogen inlet to the buffer tank (which is designed for the purpose of providing more stable pressure), one (Shanghai Regulator Co., YQD-6) is capable of providing pressures ranging from 0–1.6 MPa and another one (Linhai Pressure Gauge Co., 370) is capable of providing pressures ranging from 0–6 MPa. A 2 μm microfilter (Beijing Xiongchuan Valves Manufacture Co., SS-2210-3) is placed before the buffer tank to make sure that no dust enters the tank. It is possible that the dissolved gas in water will be released under high pressures and influences the flow characteristics. Thus, the deionized water is degassed and stored in the air-tight reservoir. The reservoir and test section are connected by a 316 SS tube (inner diameter 3 mm) which is wound into a series of circles and immersed into the constant temperature bath. The end of the tube (between the constant temperature bath and test section) is covered with thick thermal insulating foam. As the stable nitrogen is fed into the reservoir, the water is forced to flow through the constant temperature bath and then enter the test section.

The test section contains the test microtube as well as the equipments which are necessary for the measurement of inlet and outlet temperatures, pressure drop and mass flow rate. Another 2 μm microfilter (Beijing Xiongchuan Valves Manufacture Co., SS-223-3) is placed before the test section to eliminate any particles and break bubbles. Three types of test microtubes are used in this study, SS microtube (Valco Instruments Co.), PEEK microtube (Valco Instruments Co.), and FS microtube (SGE Analytical Science Pty.). The diameters of these microtubes vary from 44.5–1011 μm. Some microtubes with similar diameters are used to testify the reliability of the experiment. At the inlet and outlet of the tested microtube, two sumps are fabricated to connect the tube. As mentioned in our previous work,[59] any insertion type measurement methods have an effect on the flow characteristics in the microtube. It is a difficult task to measure the fluid temperature in a microtube. Thus, in our work as well as some other studies in the literature,[56,60–63] sumps are used to install thermal resistances and pressure transducer. The detailed structure of the sumps can be found in our previous work.[59] The sumps and test microtubes are covered with thick thermal insulating foam. Two Pt100 resistance temperature detectors (RTDs, SMWZPM-201) with an accuracy of $\pm$0.1 K are embedded at the inlet and outlet sumps to measure the inlet and outlet temperatures of the fluid. The data is acquired from the RTDs via a digital acquisition system (Advantech, USB 4718) and recorded using a computer. The maximum difference between inlet and outlet temperatures is less than 1 K. Thus, the average of the inlet and outlet temperatures is used to represent the fluid temperature just as the literature.[38,40,62,64–67] A pressure transducer (Rosemount 2051T) with an accuracy of 0.075% is embedded at the inlet sump to measure the inlet pressure. As the outlet pressure is kept at the atmospheric pressure (the outlet sump is connected to the atmosphere), the inlet pressure value equals the pressure drop across the microtube. Thus, the value of inlet

Table 5. Dimensions of All the Tested Microtubes

No.	Material	Length L (mm)	Inlet Diameter D_{in} (μm)	Outlet Diameter D_{out} (μm)	Diameter D (μm)	Roughness ε (μm)	Relative Roughness $\varepsilon \cdot D^{-1}$ (%)
1	SS	1830	1011	1012	1011	0.2	0.02
2	SS	1000	776	776	776	1.8	0.23
3	SS	500	523	524	523	2.2	0.42
4	SS	500	526	526	526	2.1	0.40
5	PEEK	500	532	529	530	0.1	0.02
6	SS	200.0	280	279	279	2.5	0.90
7	SS	200.0	254	255	255	2.7	1.06
8	SS	200.0	262	263	263	2.6	0.99
9	SS	200.0	261	261	261	3.0	1.15
10	PEEK	200.0	261	260	260	0.1	0.04
11	FS	200.0	257	255	256	0.1[a]	0.04
12	PEEK	100.0	141.1	139.9	140.5	0.1[b]	0.07
13	SS	100.0	120.4	120.2	120.3	5.2	4.32
14	SS	100.0	122.0	121.6	121.8	3.3	2.71
15	SS	100.0	120.7	120.7	120.7	3.5	2.90
16	SS	100.0	120.6	120.7	120.6	4.5	3.73
17	SS	100.0	120.4	121.0	120.7	4.0	3.31
18	PEEK	69.5	102.6	102.3	102.5	0.1[b]	0.10
19	PEEK	40.0	75.4	75.1	75.3	0.1[b]	0.13
20	PEEK	24.0	44.7	44.3	44.5	0.1[b]	0.22

SS, PEEK, and FS stand for stainless steel, poly-ether-ether-ketone, and fused silica, respectively.
[a]The roughness is decided according to literature values.
[b]The roughness is decided according to the measured roughness values of the same type (PEEK) of microtubes and literature values.

pressure is used to represent the pressure drop along the microtube as well as other references.[23,62,64,68] Both the RTDs and pressure transducer are calibrated. When the experiment begins, particular attention is paid to remove air from the whole test section, especially the two sumps (trapped air will influence the measurement of temperatures and pressures). Then, when the pressure and temperature values do not change any further, the flow is considered to have reached a steady state. A conical flask is used to collect the water from the outlet sump for certain minutes or seconds and an analytical balance (Shanghai Precision Scientific Instrument Co., JA5003B) with an accuracy of 0.001g is used to measure the mass of the collected water. There shows no detectable evaporation for water during the collecting period, which is consistent with references[23,24,35,37,62,64,68–72] that have applied the same method. The ratio of mass to time is the mass flow rate.

Dimensions of microtubes

There are totally 20 microtubes which have been tested, including 13 SS microtubes (120.3–1011 μm), 6 PEEK microtubes (44.5–530 μm), and 1 FS microtube (256 μm). The details of the dimensions of all the tested microtubes are listed in Table 5. A vernier caliper with a precision of 0.02 mm is used to measure the length of microtubes with their length less than or equals 200 mm and a meter ruler with a precision of 0.5 mm is used to measure the length of microtubes with their length larger than 200 mm.

The precise measurement of microtube diameter is one of the most significant factors that determine the accuracy of this work. Technically, it is impossible to measure the "real" diameter directly. Researchers adopted different methods to obtain an approximate value of the diameter. Weight method can be used to obtain the average diameter along the microtube. Yang et al.[49] used weight method for tubes larger than 1.1 mm. They filled mercury into the tube and measured the weight of the mercury (the weight difference between the tube with mercury inside and the tube) to obtain the volume of the mercury. Then the average diameter could be obtained according to the length of tube. There are several factors that contribute to the uncertainty in diameter measurement with weight method. The most important factor is the fill of mercury. Considering the fact that it is more difficult to fully fill mercury into smaller microtubes, the weight method may be less accurate for microtubes with smaller diameter. Besides, the mercury weight and density will also have effect on the accuracy of diameter measurement. Krishnamoorthy and Ghajar[73] (published in 2007) concluded that almost 15 out of 23 researchers used scanning electron microscope (SEM) method for accurate diameter measurement. As for the studies reported after 2007, almost all the researchers used SEM method to measure microtube diameter. SEM method utilizes a SEM to obtain the image of cross section of the microtube (with a known pixel-to-length scale on the image). Then the SEM measurement software is used to calculate the diameter according to the scale. The uncertainty in diameter measurement with SEM method is also comprised of several contributions. First, the SEM itself owns a measurement uncertainty. Then, the diameter obtained through the SEM method can only represent the diameter of one cross section instead of an average value. The accuracy of diameter value can be affected if the diameter varies along the microtube. Moreover, there may be some human bias in the calculation, which is difficult to quantify. Thus, as much as possible calculations on one image should be performed to diminish the human bias as far as possible.

In our previous work,[59,74,75] we have performed experiments (comparison between the diameters measured by the weight method and SEM method) for microtubes with diameter larger than 250 μm to verify that the diameters can be assumed to be uniform along the microtube. Hence, SEM method is used in this work and only the diameters of both ends of the microtubes are measured in this work, just the same as some other studies in the literature.[64,65,76] A thermal field emission SEM (FEI, SIRION-100) is used to measure the diameters of microtubes. A verification regulation for analytical SEM (JJG Education Office 010-1996) is acquired to calibrate the SEM using the same SEM acceleration

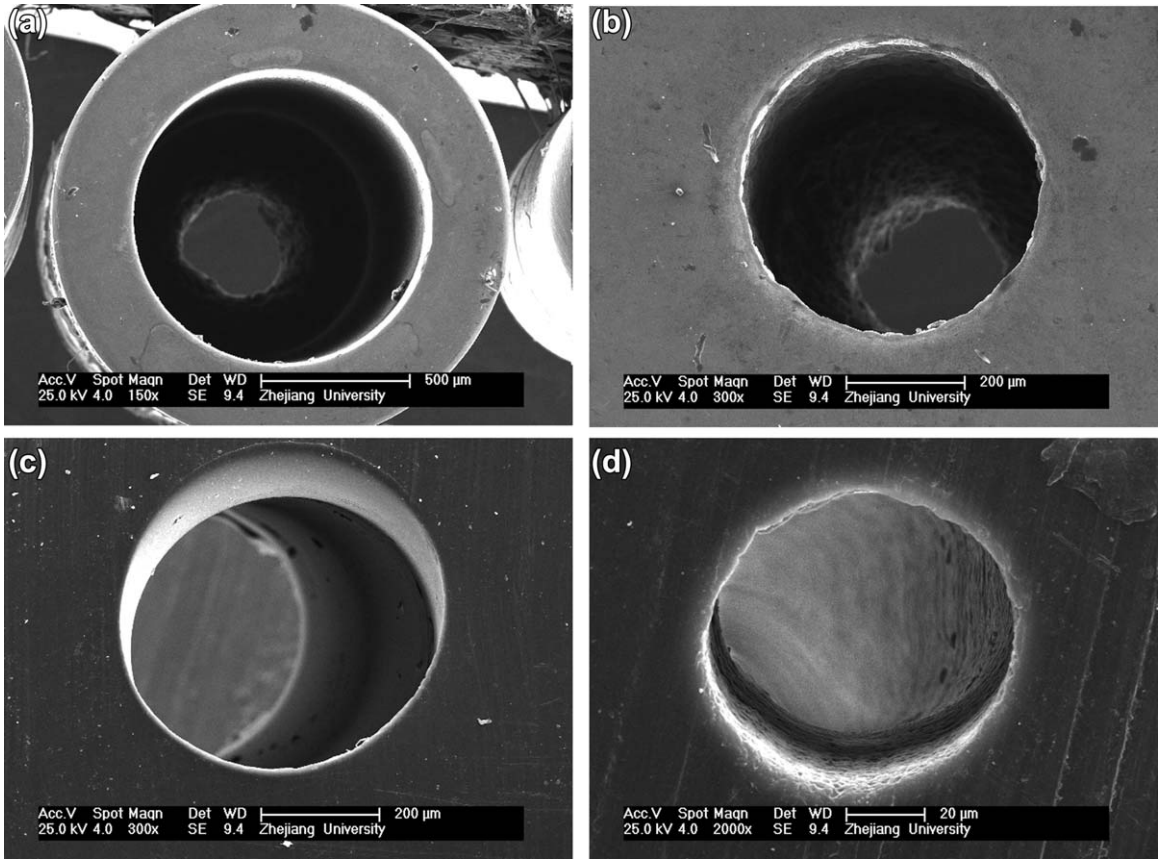

Figure 2. Diameter images of one end of tested microtubes, (a) SS1011, (b) SS523, (c) PEEK530, and (d) PEEK75.3.

(SS and PEEK stand for stainless steel and poly-ether-ether-ketone, respectively, the number stands for the diameter of tested microtube).

voltage and magnifications as that used for the diameter measurement of microtubes. The accuracy of the SEM is found to be around 0.5%. All the microtubes are washed in an ultrasonic cleaner before the measurement. The PEEK microtubes are sputter-coated with gold to be electric and make sure that clear images of diameters are obtained. Once images of diameters have been captured, the SEM software is used to calculate the diameter. The diameter images of one end of tested microtubes SS1011 (SS stands for the material of microtube and 1011 stands for the diameter of microtube, similarly hereinafter), SS523, PEEK530, and PEEK75.3 are shown in Figure 2 and all the diameter images of both ends of the 20 tested microtubes are shown in the Supporting Information Figure S1. Ten calculations of one image are averaged to minimize the human bias. As can be observed in Table 5, the maximum deviation of the diameters for the two ends is 0.9% and the average absolute deviation (AAD) for all microtubes is 0.3%. Thus, the average diameter of the two ends (20 calculations) is calculated to represent the diameter of the microtube just as other literature.[64,65,76] The precision of the diameter values obtained in this work is around 1.00% considering all the contributions.

An optical profiler (Veeco Instruments, Wyko NT9100, precision ± 0.1 μm) which is capable of noncontact, three-dimensional measurements is used to measure the surface roughness of microtubes. Average roughness (R_a) and root mean square roughness (R_q) can be obtained. According to references,[25,26,67,76–78] average roughness (R_a) is chosen to represent the roughness (ε) of microtubes. The microtubes are sanded for the purpose of having their inner surface revealed and then washed in an ultrasonic cleaner before the measurement. PEEK and FS microtubes can be easily obtained and are always regarded as smooth microtubes in literature.[22,26,32,62,79–81] Thus, only two pieces of six PEEK microtubes are chosen to have the roughness measured and measurements are taken from four different sections of each microtube. The value of the measured roughness of PEEK microtubes is in the range 0.0–0.2 μm and is averaged to 0.1 μm, which is in accordance with the literature value.[22,26] For the roughness of FS microtube, literature value[32,62,79,80] is in the range 0–70 nm. So the roughness of FS microtube is rounded to 0.1 μm in this work. As for the 13 SS microtubes, surface roughnesses are taken from six different sections of each microtube. The detailed roughness images of every section of 13 SS and 2 PEEK microtubes are shown in Supporting Information Figure S2. The average roughness of each microtube is listed in Table 5 and the roughness images of one section of tested microtubes SS1011, SS523, SS120.3, and PEEK530, are shown in Figure 3.

Mathematical formulations

The fluid temperature (T), pressure drop (ΔP), and mass flow rate (M) are obtained through the experiment. The density (ρ) and viscosity (η) of water are calculated according to fluid temperature. Thus, the Reynolds number (Re) can be calculated as follows

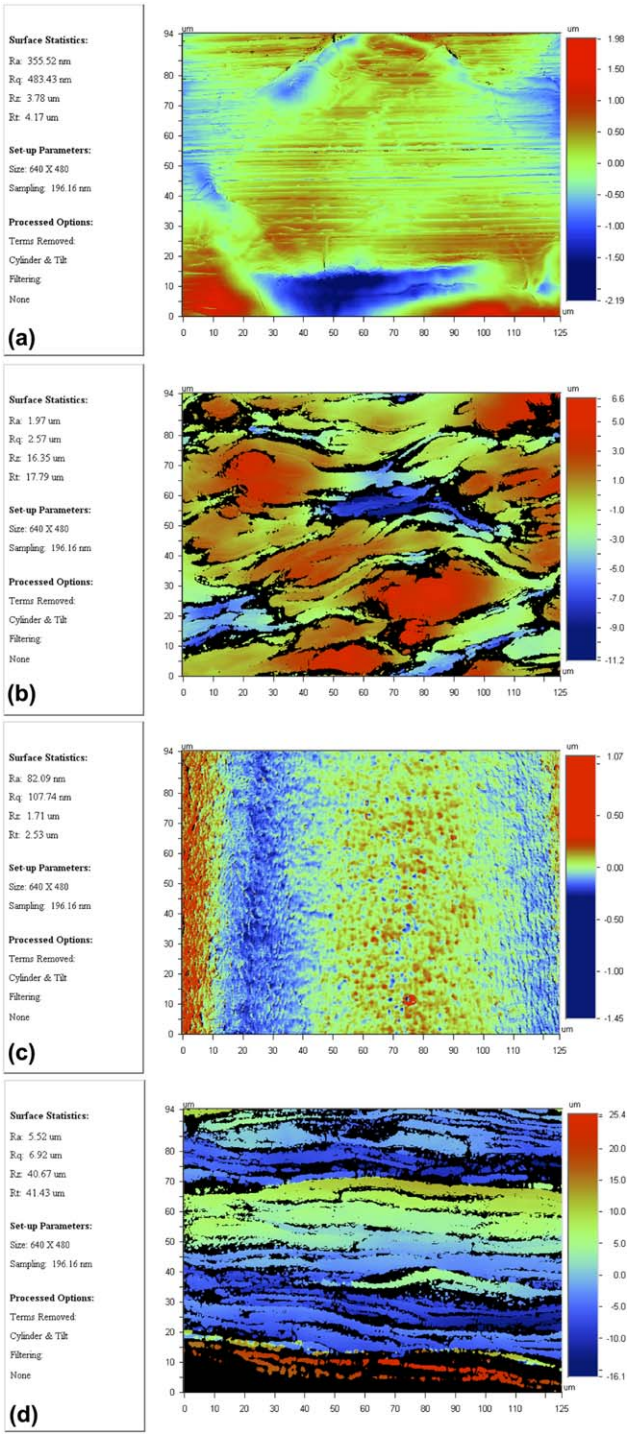

Figure 3. Roughness images of one section of tested microtubes (a) SS1011, (b) SS523, (c) PEEK530, and (d) SS120.3.

(SS and PEEK stand for stainless steel and poly-ether-ether-ketone, respectively, the number stands for the diameter of tested microtube). [Color figure can be viewed in the online issue, which is available at wileyonlinelibrary.com.]

$$\mathrm{Re}=\frac{4M}{\pi\eta D} \tag{1}$$

The friction factor (f) can be obtained according to Eq. 2

$$f=\frac{\Delta P_{\mathrm{FD}}\pi^2D^4\rho}{8M^2}\frac{D}{L} \tag{2}$$

where ΔP_{FD} is fully developed flow pressure drop and can be calculated as

$$\Delta P_{\mathrm{FD}}=\Delta P-\Delta P_{\mathrm{in}}-\Delta P_{\mathrm{D}}-\Delta P_{\mathrm{out}} \tag{3}$$

where ΔP_{in} is pressure losses due to the abrupt contraction in the inlet, ΔP_{D} is pressure losses in hydrodynamic development flow (unfully developed flow in the entrance part), and ΔP_{out} is pressure losses due to the abrupt extension in the outlet. ΣK_{L} is used to represent the additional pressure losses as follows[23,24,40,46,57,58,60,62–65,82]

$$\Delta P_{\mathrm{in}}+\Delta P_{\mathrm{D}}+\Delta P_{\mathrm{out}}=\Sigma K_L\frac{8M^2}{\pi^2D^4\rho} \tag{4}$$

Combining Eqs. 2–4, friction factor can be calculated as

$$f=\left(\frac{\Delta P\pi^2D^4\rho}{8M^2}-\Sigma K_L\right)\frac{D}{L} \tag{5}$$

where ΣK_{L} can be expressed in different ways. Different references[23,24,40,46,57,58,60,62–65,82] gave different expressions of ΣK_{L}. For example, Li et al.[23,62] suggested that ΣK_{L} equaled 2.36, Judy et al.[64] pointed out that ΣK_{L} equaled 3.1, and Ergu et al.[24] thought that ΣK_{L} should be calculated by a complex expression. As it is difficult to define a specific value of ΣK_{L}, some researchers proposed other methods to eliminate the additional pressure losses. Researchers[22,71,72,77] who used wide channels placed pressure taps far away from the inlet and outlet for the purpose of measuring the pressure drop of fully developed flow directly. However, it is difficult for microtubes to copy this method without disrupting the flow.[29,70] Some other researchers[20,29,48,69,70] utilized a short and a long microtube method. Thus, ($\Delta P_{\mathrm{long}}-\Delta P_{\mathrm{short}}$) represents the pressure drop of fully developed flow over the tube length ($L_{\mathrm{long}}-L_{\mathrm{short}}$). However, it is impossible to find a short and a long microtube sharing the exactly same diameter and surface roughness. Even the microtubes which are bought in a same batch from a same corporation will not be accurately uniform. In a word, it is impossible to find a perfect method which could totally eliminate errors. Thus, we choose to follow the most simple and typical method,[40,58,60,63,83] that is, perform experiments in long enough microtubes to neglect the hydrodynamic development flow and define that

$$\Delta P_{\mathrm{in}}+\Delta P_{\mathrm{out}}=1.5\frac{8M^2}{\pi^2D^4\rho} \tag{6}$$

Thus, Eq. 5 can be simplified to Eq. 7

$$f=\left(\frac{\Delta P\pi^2D^4\rho}{8M^2}-1.5\right)\frac{D}{L} \tag{7}$$

and Poiseuille number (fRe) can be expressed as

$$f\mathrm{Re}=\left(\frac{\Delta P\pi^2D^4\rho}{8M^2}-1.5\right)\frac{4M}{L\pi\eta} \tag{8}$$

Uncertainty analysis

Understanding the experimental uncertainty of calculated Reynolds number (Re), friction factor (f), and Poiseuille number (fRe) is necessary. According to error propagation

Table 6. Uncertainty in Measured and Calculated Items

Items	$\delta M/M$	$\delta\eta/\eta$	$\delta D/D$	$\delta\Delta P/\Delta P$	$\delta\rho/\rho$	$\delta L/L$	δRe/Re	$\delta f/f$	δfRe/fRe
Uncertainty (%)	0.1	1	1	0.075	0.01	0.1	1.42	5.01	4.13

technique[64,84] and Eqs. 1, 7, and 8, the uncertainty in Re, f, and fRe can be expressed as

$$\frac{\delta \mathrm{Re}}{\mathrm{Re}} = \left[\left(\frac{\delta M}{M}\right)^2 + \left(\frac{\delta \eta}{\eta}\right)^2 + \left(\frac{\delta D}{D}\right)^2 \right]^{1/2} \tag{9}$$

$$\frac{\delta f}{f} = \left[\left(\frac{\delta \Delta P}{\Delta P}\right)^2 + \left(5\frac{\delta D}{D}\right)^2 + \left(\frac{\delta \rho}{\rho}\right)^2 + \left(2\frac{\delta M}{M}\right)^2 + \left(\frac{\delta L}{L}\right)^2 \right]^{1/2} \tag{10}$$

$$\frac{\delta f\mathrm{Re}}{f\mathrm{Re}} = \left[\left(\frac{\delta M}{M}\right)^2 + \left(\frac{\delta \eta}{\eta}\right)^2 + \left(4\frac{\delta D}{D}\right)^2 + \left(\frac{\delta \Delta P}{\Delta P}\right)^2 + \left(\frac{\delta \rho}{\rho}\right)^2 + \left(\frac{\delta L}{L}\right)^2 \right]^{1/2} \tag{11}$$

where $\delta M/M$, $\delta\eta/\eta$, $\delta D/D$, $\delta\Delta P/\Delta P$, $\delta\rho/\rho$, and $\delta L/L$ mean uncertainty in mass flow rate, viscosity, diameter, pressure drop, density, and length. Attempts have been made to reduce the experimental uncertainty in these items as far as possible. A detailed description of the contributions to the uncertainty in diameter is given above and the uncertainty is approximately 1%. The uncertainty in mass flow rate results from the 0.001 g uncertainty in mass and human bias in timekeeping, and is estimated to be less than 0.1%. The uncertainties in viscosity and density result from 0.1–0.5 K uncertainty in temperature and are estimated to be less than 1 and 0.01%, respectively. The uncertainty in pressure drop is given by the manufacturer and the uncertainty in length is determined by the vernier caliper and meter ruler. The details of uncertainty are listed in Table 6.

Results and Discussion

Experimental results

The experimental results of f versus Re relationship (in the log–log plot) for tested microtubes SS1011, SS523, SS120.3, and PEEK140.5 are shown as representative in Figure 4 (results of all the 20 tested microtubes are shown in Supporting Information Figure S3). On the whole, the tendency of f versus Re relationship for microtubes is approximately the same as conventional sized tubes. In the laminar flow region ($\mathrm{Re} < \mathrm{Re_c}$, $\mathrm{Re_c}$ is the critical Reynolds number), the friction factor decreases linearly with the increase of Reynolds number (in the log–log plot) and the Poiseuille number keeps constant as Reynolds number increases. At critical Reynolds number ($\mathrm{Re} = \mathrm{Re_c}$), a transition from laminar to turbulent flow starts. After that, f versus Re relationship (in the log–log plot) is not in linear relation anymore and the Poiseuille number rises with the increase of Reynolds number ($\mathrm{Re_c} < \mathrm{Re} < \mathrm{Re_t}$, $\mathrm{Re_t}$ is the Reynolds number where turbulent flow begins). Attention should be paid that the critical Reynolds number is defined as the point that

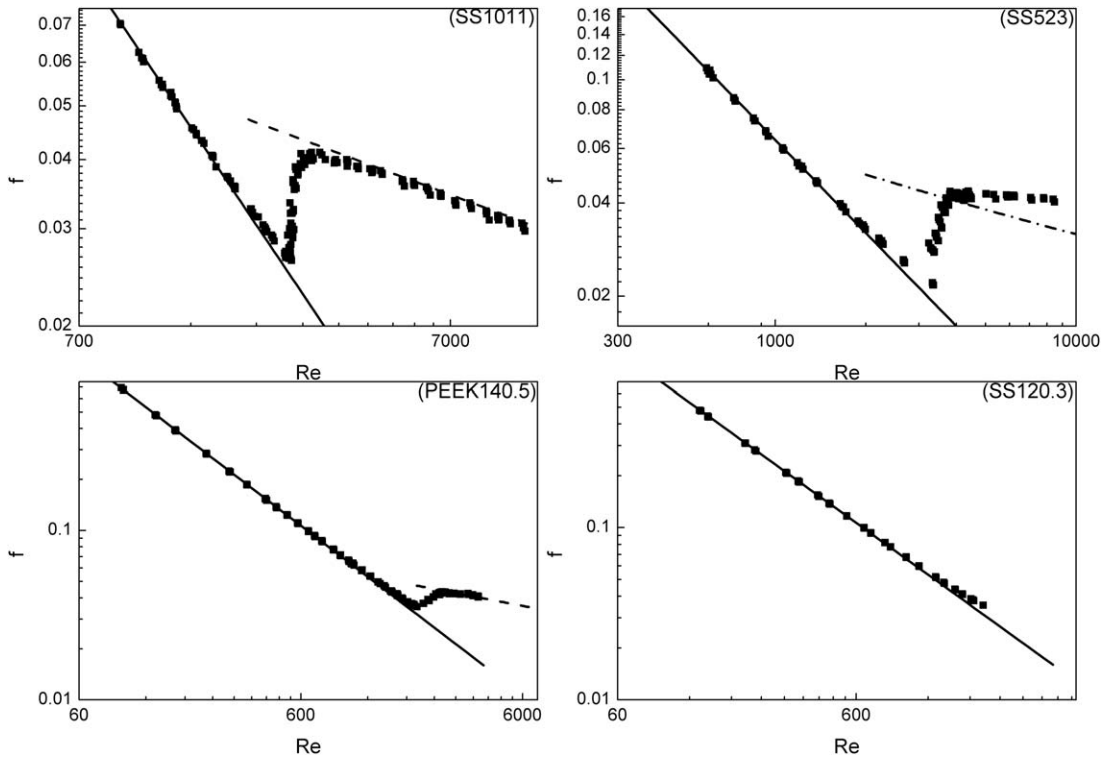

Figure 4. The experimental results of friction factor (*f*) versus Reynolds number (Re) relationship for tested microtubes SS1011, SS523, PEEK140.5, and SS120.3, solid line, Hagen-Poiseuille equation, dash line, Blasius equation, dash dot line, Moody equation.

(SS and PEEK stand for stainless steel and poly-ether-ether-ketone, respectively, the number stands for the diameter of tested microtube).

Table 7. The Detailed Experimental Results Including Ranges of Experimental Reynolds Number Re, Ranges of Experimental Friction Factor *f*, Average Poiseuille Number *f*Re of Laminar Flow, Critical Reynolds Number Re_c, and Reynolds Number Where Turbulent Flow Begins Re_t

Tested microtubes	Re range	*f* range	$(fRe)_{laminar,ave}$	Re_c	Re_t
SS1011	903–11101	0.0263–0.0705	64	2009	3113
SS776	1073–11644	0.0265–0.0599	64	1957	2933
SS523	591–8473	0.0217–0.1093	64	1496	4004
SS526	748–8645	0.0192–0.0853	64	1518	4052
PEEK530	404–4759	0.0345–0.1596	64	1544	2553
SS279	303–5452	0.0251–0.2104	64	1321	3340
SS255	169–4534	0.0252–0.3746	63	1336	3200
SS263	167–4646	0.0227–0.3805	63	1331	3455
SS261	237–4611	0.0211–0.2703	64	1315	4048
PEEK260	159–4658	0.0343–0.4013	64	1331	2612
FS256	232–4605	0.0322–0.2770	64	1306	2793
PEEK140.5	93–3793	0.0357–0.5858	64	939	2595
SS120.3	132–2041	0.0355–0.4817	64	817	–
SS121.8	101–2068	0.0358–0.6268	64	849	–
SS120.7(No 15)	142–2007	0.0369–0.4463	64	836	–
SS120.6	129–2033	0.0365–0.4937	64	809	–
SS120.7(No 17)	134–2113	0.0362–0.4761	64	799	–
PEEK102.5	109–2280	0.0354–0.6927	63	680	–
PEEK75.3	44–1973	0.0358–1.4476	64	494	–
PEEK44.5	29–656	0.1024–2.2084	64	302	–

SS, FS, and PEEK stand for stainless steel, fused silica, and poly-ether-ether-ketone, respectively, the number stands for the diameter of tested microtube, No 15 and No 17 are the numbers of microtubes listed in Table 5.

friction factor starts to deviate from the linear portion of *f* versus Re plot in laminar flow region, that is, the point that Poiseuille number begin to rise with the increase of Reynolds number, in the present work as well as other literature,[22,23,38,39,41–43] not the point that friction factor starts to increase as the increase of Reynolds number. When the Reynolds number becomes larger ($Re > Re_t$), the friction factor decreases slowly with the increase of Reynolds number. This is the turbulent flow region. Similarly, the experimental results of other tested microtubes can be divided into the three regions, the laminar flow region, transitional flow region and turbulent flow region. As can be observed in Figure 4, for the microtubes with diameter $\geq$140.5 μm, laminar, transitional, and turbulent flows are studied, while for microtubes with diameter $<$140.5 μm, the current experimental facility and methods limit the experimental Reynolds number to be less than 2280 and only laminar and beginning of transitinal flows are studied.

A total of 2502 data points (687, 1277, and 538 data points for laminar, transitional, and turbulent flow, respectively) were obtained over the Reynolds number range 29–11,644 (the detailed data which include density (ρ) and viscosity (η) of water, mass flow rate (M), pressure drop (ΔP), Reynolds number (Re), friction factor (f), and Poiseuille number (fRe) of 2502 data points for all the 20 tested microtubes are listed in Supporting Information Tables S1-20). The experimental results as well as ranges of experimental Reynolds number (Re), ranges of experimental friction factor (f), average Poiseuille number (fRe) of laminar flow, critical Reynolds number (Re_c), and Reynolds number where turbulent flow begins (Re_t) are listed in Table 7. Differences of liquid flow characteristics between microtubes and conventional sized tubes can be observed from Table 7. The flow characteristics are discussed in detail in the following passages.

Laminar flow region

The experimental results of *f* versus Re relationship of all the tested microtubes in the laminar flow region are shown in Supporting Information Figure S3. The experimental friction factor and Reynolds number have an almost linear trend as predicted by the conventional theory of Hagen–Poiseuille for the laminar flow. The corresponding enlargement of experimental results of fRe versus Re plot of all the tested microtubes in laminar flow region are shown in Figure 5. The experimental values of Poiseuille number are seen to keep constant as Reynolds number increases (in the laminar flow region) within measurement error. For each tested microtube, the average of all the Poiseuille number in laminar flow region ($(fRe)_{laminar,ave}$) is calculated and listed in Table 7. Almost all the laminar flow data nicely lay next to the average value 64. This finding is in accordance with the recent researches.[25–30] Therefore, conclusion can be made that to the degree of the current experimental uncertainties, the Poiseuille number values agree well with theoretical predictions (fRe equals the constant 64) for microtubes with diameters in the range 44.5–1011 μm and roughness (relative roughness) less than 5.2 μm (4.32%).

Critical Reynolds number

Critical Reynolds number is the indicator of the transition from laminar to turbulent flow and the investigation on critical Reynolds number is meaningful. Researches on critical Reynolds number goes back to 1883 when Osborne Reynolds found that a laminar flow becomes unstable if the dimensionless number (which is named after him now) exceeds a certain critical value. However, his finding still has not been explained satisfactorily by theory[85,86] and research on the critical Reynolds number mainly relies on experimental results.

To figure out whether early transition occurs in microtubes and what is the cause of early transition, the specific value of critical Reynolds number should be first obtained using an appropriate mathematical method. Unfortunately, most of the references[18,23,35–40] did not mention how they obtained the values of critical Reynolds number. A few references[42,43] considered the Reynolds number where the deviation from the linear portion of the *f* versus Re in the log–log plot achieved

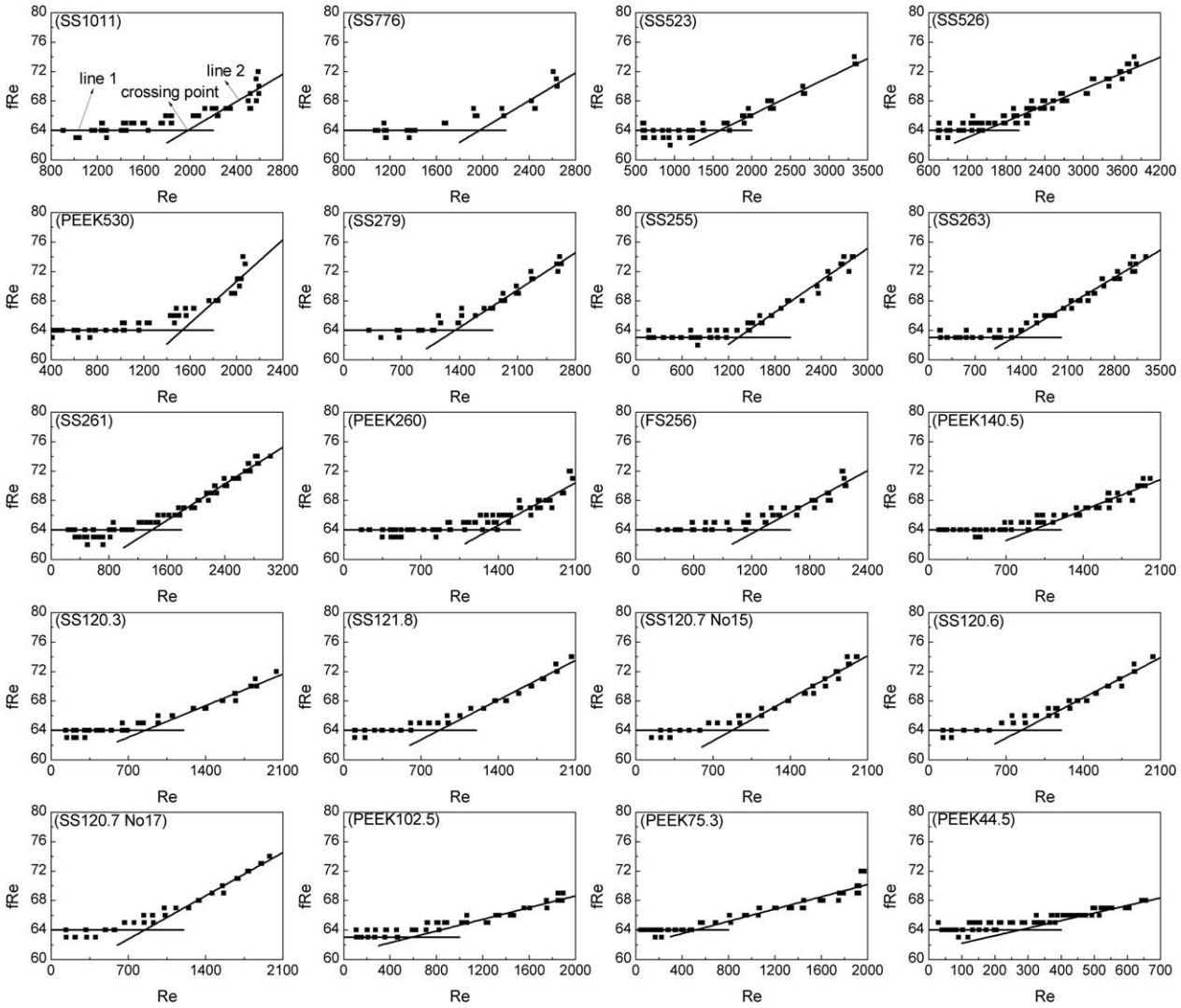

Figure 5. The experimental results of Poiseuille number (*f*Re) versus Reynolds number (Re) relationship in laminar flow region and beginning of transitional region and calculation results of critical Reynolds number for all the 20 tested microtubes.

(SS, FS, and PEEK stand for stainless steel, fused silica, and poly-ether-ether-ketone, respectively, the number stands for the diameter of tested microtube, No 15 and No 17 are the numbers of microtubes listed in Table 5).

some certain values, such as 1[42] or 5%,[43] as the critical Reynolds number. It seems like that the deviation criterion is difficult to determine. In that case, a specific definition to calculate critical Reynolds number was proposed in this work.

Figure 5 shows the experimental results of *f*Re versus Re relationship in laminar flow region and beginning of transitional flow region for all the 20 tested microtubes. As can be observed in Figure 5, the Poiseuille number keeps constant as the increase of Reynolds number in laminar flow region. Then, the Poiseuille number increases with the increase of Reynolds number when the Reynolds number is larger than critical Reynolds number. The tendency of *f*Re versus Re relationship after critical Reynolds number is different from that before critical Reynolds number. Since the Poiseuille number is a continuous function of Reynolds number, the critical Reynolds number should be located on the crossing point of two trend lines. The calculation process of critical Reynolds number of SS1011 is given as an example (shown in Figure 5). First, the approximate location of the critical Reynolds number is obtained and it is among 1800–2200 for SS1011 (the deviation of *f*Re from the Poiseuille number in laminar flow region 64 is larger than the uncertainty 4.13% among 1800–2200). Second, line 1 (horizontal line: *f*Re = average value of Poiseuille number in laminar flow region) which represents the tendency of the data in laminar flow region is obtained. Thirdly, line 2 (a linear regression line of the data points which are larger than 2200) which represents the tendency of the beginning of transitional *f*Re versus Re relationship is obtained. Finally, the crossing point of the two lines represents the value of critical Reynolds number. The deviation between the linear regression equations and experimental data is in the range 0.3–1.1% and the AAD was found to be 0.6% for all the 20 tested microtubes. Thus, considering the uncertainty in experiment and calculation method, the uncertainty in critical Reynolds number is approximately 2%.

The calculation results, two lines and their crossing point, for all the 20 tested microtubes are also shown in Figure 5. The specific values of critical Reynolds number are listed in Table 7. For the tested tube with the greatest diameter

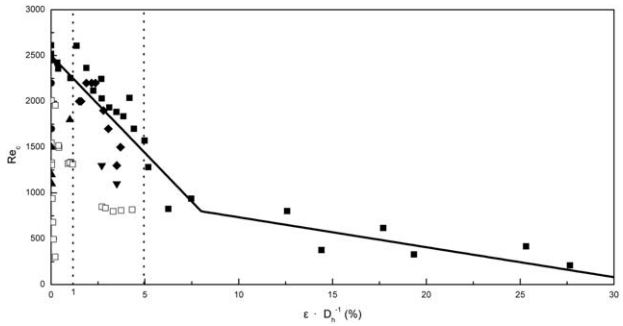

Figure 6. The relationship between critical Reynolds number (Re_c) and relative roughness ($\varepsilon \cdot D_h^{-1}$) based on literature data, ■, Kandlikar,[41,42] ●, Pfund et al.,[22] ▲, Zhao and Liu,[39] ▼, Liu et al.,[38] ◆, Ghajar et al.,[43] and □, experimental data in this work, solid line, Kandlikar's correlation.

1011 μm (which belongs to conventional scale based on the microscale definition), the critical Reynolds number value is 2009, which fits well with the critical Reynolds number value (2000) for conventional sized tube[23,31,32,34,35,40,64] within the uncertainty (2%) and also verifies the validity of this work. For the tested microtube with 776 μm diameter, the critical Reynolds number value is 1957 and is a little lower than the value 2000. With the further decrease of microtube diameters, the values of critical Reynolds number decrease. The critical Reynolds number is in the range of 302–1957 for microtubes with diameters varing from 44.5–776 μm. It is obvious that early transition happened in microtubes. This phenomenon of early transition is also observed by other literature.[18,22,23,35–43]

As far as now, there are two viewpoints in literature discussing the factors that may lead to an early transition. Some researchers[18,22,39,43] concluded that the critical Reynolds number decreased with decreasing diameter, while some other researchers[40–42] believed that it was the increase of roughness led to lower critical Reynolds number. Kandlikar is one of the most representive researchers that considered the critical Reynolds number affected by roughness. They[41,42] proposed Eqs. 12 and 13 based on their own data to calculate the critical Reynolds number.

$$0 \le \varepsilon/D_{h,cf} \le 0.08 \quad \mathrm{Re}_{c,cf} = \mathrm{Re}_0 - \frac{\mathrm{Re}_0 - 800}{0.08}\left(\frac{\varepsilon}{D_{h,cf}}\right) \quad (12)$$

$$0.08 \le \varepsilon/D_{h,cf} \le 0.15 \quad \mathrm{Re}_{c,cf} = 800 - 3270\left(\frac{\varepsilon}{D_{h,cf}} - 0.08\right) \quad (13)$$

where $Re_{h,cf}$ is critical constricted Reynolds number, ε is roughness, $D_{h,cf}$ is constricted hydraulic diameter, and Re_0 is critical Reynolds number for $\varepsilon \cdot D_{h,cf}^{-1} = 0$. The AAD was found to be 13% for the 27 experimental data points.

However, though Eqs. 12 and 13 work well for Kandlikar's[41,42] own experimental data, Zhou and Yao[87] pointed out that Kandlikar's correlation poorly described other random roughness or other types of microchannels in literature. To verify whether Kandlikar's correlation was applicative, a careful collection of experimental data, including the related diameter, relative roughness and critical Reynolds number, was performed in this work. Though a number of references mentioned critical Reynolds number, there were only limited references[18,22,31,34,38,39,43] that gave the specific values of critical Reynolds number according to different dimensions of microtubes (or microchannels). References that did not list specific values of critical Reynolds number according to corresponding dimensions were not included in this collection. The specific values of critical Reynolds number together with the relevant diameter and relative roughness of references are listed in Supporting Information Table S21, attached with the detailed description on the methods to obtain the data sets. Experimental critical Reynolds number in this work and references[22,38,39,43] are shown in Figure 6, compared with Kandlikar's correlation (and Kandlikar's experimental data). As can be observed in Figure 6, the deviation between Kandlikar's correlation and experimental data sets in this work and references[22,38,39] (over 30%) is quite large. Kandlikar mainly focused on the study of microchannels with large roughness (e.g., 17.0[41] and 23.19 μm[42] and large relative roughness (e.g., 14[41] and 28%[42] while the roughness and relative roughness of most of microtubes (or microchannels) used in references[18,22,31,34,38,39] and this work was less than 10 μm and 5.00%. The roughness may have large effect on critical Reynolds number when it is quite large. However, the effect of roughness might be tiny when the roughness is less than 5.00% and that might explain the reason why Kandlikar's correlation poorly described other reference data since Kandlikar's correlation is based on the effect of roughness. As also can be observed in Figure 6, though the critical Reynolds number decreases with the increase of relative roughness roughly for microtubes with relative roughness larger than 1.00%, the data of microtubes with relative roughness less than 1.00% (19 data points of critical Reynolds number, including 13 data points from this work and 6 data points from references,[18,22,39] ranging from 302–2200), clearly show that there seems no obvious relationship between relative roughness and critical Reynolds number. The reason why the critical Reynolds

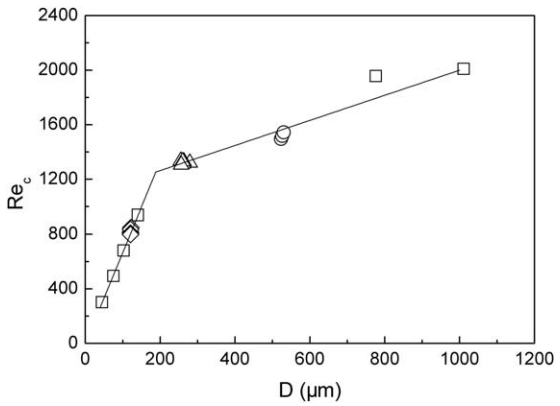

Figure 7. The relationship between critical Reynolds number (Re_c) and diameter (D), □, SS1011, SS776, PEEK140.5, PEEK102.5, PEEK75.3, PEEK44.5, ○, SS523, SS526, PEEK530, △, SS279, SS255, SS263, SS261, PEEK260, FS256, ◇, SS120.3, SS121.8, SS120.7(No 15), SS120.6, SS120.7(No 17).

(SS, FS, and PEEK stand for stainless steel, fused silica, and poly-ether-ether-ketone, respectively, the number stands for the diameter of tested microtube, No 15 and No 17 are the numbers of microtubes listed in Table 5).

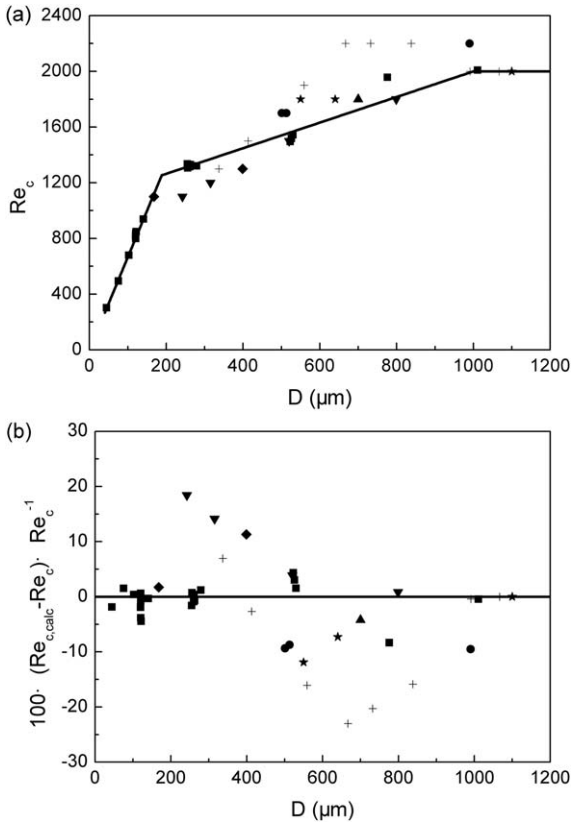

Figure 8. (a) The relationship between experimental critical Reynolds number (Re_c) and diameter (D), solid line, Eq. 15 and (b) relative deviation between experimental critical Reynolds number (Re_c) and calculated critical Reynolds number ($Re_{c,calc}$) which is obtained through Eq. 15: ■, this work, •, Pfund et al.,[22] ▲, Agostini et al.,[31] ▼, Zhao and Liu,[39] ◆, Liu et al.,[38] ⋆, Dutkowski,[34] +, Ghajar et al.[43]

number decreases with the increase of relative roughness roughly when relative roughness is larger than 1.00% might be that for most situations, microtubes (or microchannels) with smaller diameters always have higher relative roughnesses.

Researchers who held the opinion that early transition is caused by the decrease of diameter have not came up with a relevant equation describing the relationship between critical Reynolds number and diameter, the quantitative study on the factor that leads to early transition seems to be in a lack.

In our case, for microtubes with diameter less than 1000 μm, the critical Reynolds number decreases when the diameter decreases as shown in Figure 7. The critical Reynolds number values of microtubes with diameters of 523, 526, and 530 μm ($\varepsilon \cdot D^{-1}$ 0.42, 0.40, and 0.02%) are 1496, 1518, and 1544, respectively. The microtubes with roughnesses (relative roughnesses) varying from 0.1–2.2 μm (0.02–0.42%) share similar critical Reynolds number. Similar phenomena were also observed for ~260 and ~121 μm diameter microtubes. These three data sets clearly stated that for microtubes with roughness (relative roughness) less than 5.2 μm (4.32%), the effect of roughness on the critical Reynolds number is tiny and can be ignored. It is the decrease of diameter that leads to earlier transition for microtubes with roughness (relative roughness) less than 5.2 μm (4.32%).

We think that the deviation between experimental critical Reynolds number and conventional theory (2000) can be described as a function of the deviation between microtube diameter and 1000 μm (which is usually adopted as the critical point separating microscale and conventional scale[9–13]. Thus, a parameter α was proposed to describe the characteristic of microtube as follows

$$\alpha = \frac{1000 - D}{1000} \tag{14}$$

where 1000 represents the diameter that separating microscale and conventional scale in μm, D is the diameter of tested microtubes in μm. As can be observed from Figure 7, the experimental critical Reynolds number decreases slowly with the decrease of microtube diameter when the microtube diameter is larger than 255 μm, while the experimental critical Reynolds number decreases much quicker with the decrease of microtube diameter when the microtube diameter is smaller than 140.5 μm. So, the characteristic parameter α was used to calculate the critical Reynolds number for microscale in the form of segmented function as follows

$$\mathrm{Re}_c = \begin{cases} 2000,\ 1000\,\mu\mathrm{m} \le \mathrm{D} & \text{(a)} \\ 2000 - 2000\times 0.46\alpha,\ 188\,\mu\mathrm{m} \le \mathrm{D} < 1000\,\mu\mathrm{m} & \text{(b)} \\ 2000 - 2000\times(3.33\alpha - 2.33),\ 44.5\,\mu\mathrm{m} \le \mathrm{D} < 188\,\mu\mathrm{m} & \text{(c)} \end{cases} \tag{15}$$

where Re_c is the critical Reynolds number for microscale, D is diameter of tested microtubes in μm, 188 μm is in the range of 140.5–255 μm and is determined by Eqs. 15(b) and 15(c).

The AAD between the calculated critical Reynolds number ($Re_{c,calc}$) which was obtained with Eq. 15 and experimental critical Reynolds number (Re_c) is defined as

$$\mathrm{AAD}(\%) = \frac{\sum_{i=1}^{N_p} \left|100\left(\mathrm{Re}_{c,calc} - \mathrm{Re}_c\right)/\mathrm{Re}_c\right|_i}{N_p} \tag{16}$$

where N_p represents the number of data points. The AAD is 1.9% for the 20 experimental data points in this work, with a maximum deviation of 8.3%. The new obtained Eq. 15 is shown in Figure 8a together with the experimental data. The deviation between the experimental critical Reynolds number and calculated critical Reynolds number which is obtained through Eq. 15 is shown in Figure 8b. The new Eq. 15 is also compared with data points from references (listed in Supporting Information Table S21) and shown in Figure 8a. The new correlations basically agree with the references.[22,31,34,38,39,43] The overall AAD is 5.6% with a maximum deviation of 23.0% and the detailed deviations are shown in Figure 8b.

As the roughness (relative roughness) of the microtubes used in this work is in the range of 0.1–5.2 μm (0–4.32%) and the roughness (relative roughness) of the microtubes (or microchannels) used in references[22,31,34,38,39,43] is in the range of 0.1–10 μm (0–3.70%), thus, Eqs. 15(b) and 15(c) are only for microtubes (or microchannels) with their roughness (relative roughness) smaller than or equals 10 μm (4.32%). Fortunately, most commercial available microtubes (or microchannels) own roughnesses (relative roughnesses) less than 10 μm

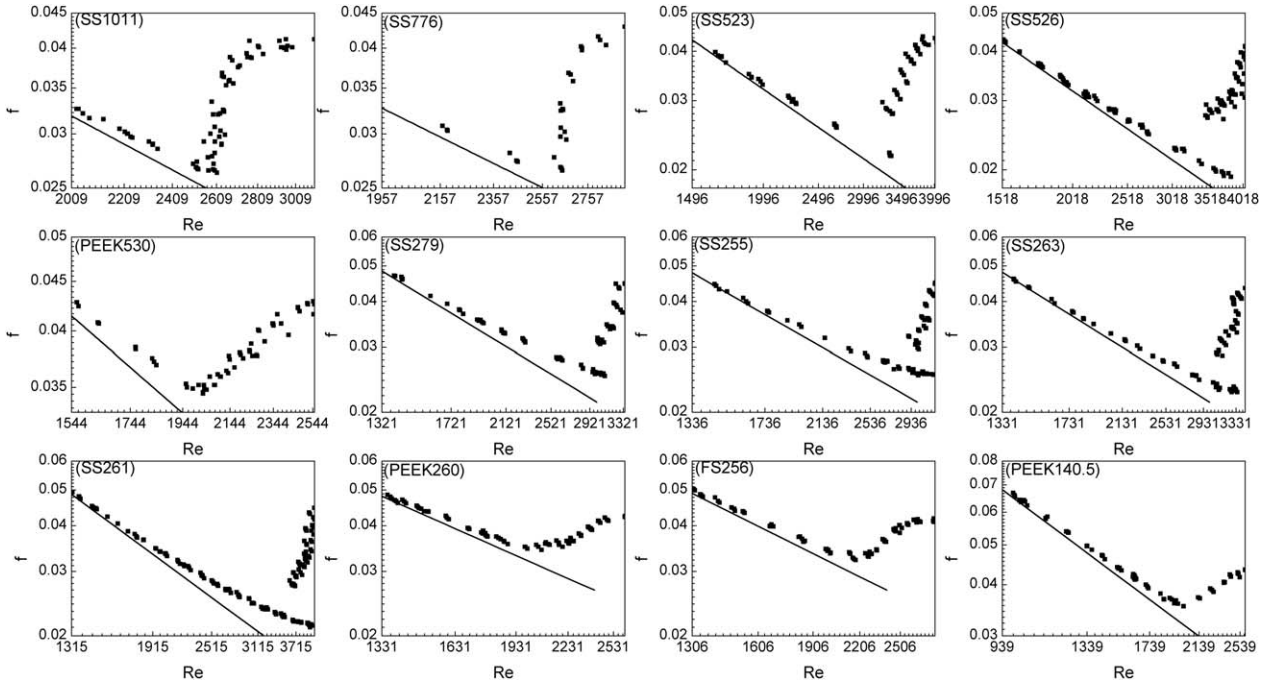

Figure 9. The experimental results of friction factor (*f*) versus Reynolds number (Re) relationship in transitional flow region (start with Re_c and end with Re_t) of the tested microtubes with diameter $\geq$ 140.5 μm, solid line, Hagen-Poiseuille equation.

(SS, FS, and PEEK stand for stainless steel, fused silica, and poly-ether-ether-ketone, respectively, the number stands for the diameter of tested microtube).

(4.32%). The roughness may play a more important role when roughness is larger than 10 μm. More researches and data are needed to obtain more precise and wide applicable correlations.

Transitional flow region

The values of Reynolds number where turbulent flow begins for each microtube were obtained using the same method for calculation of critical Reynolds number and are

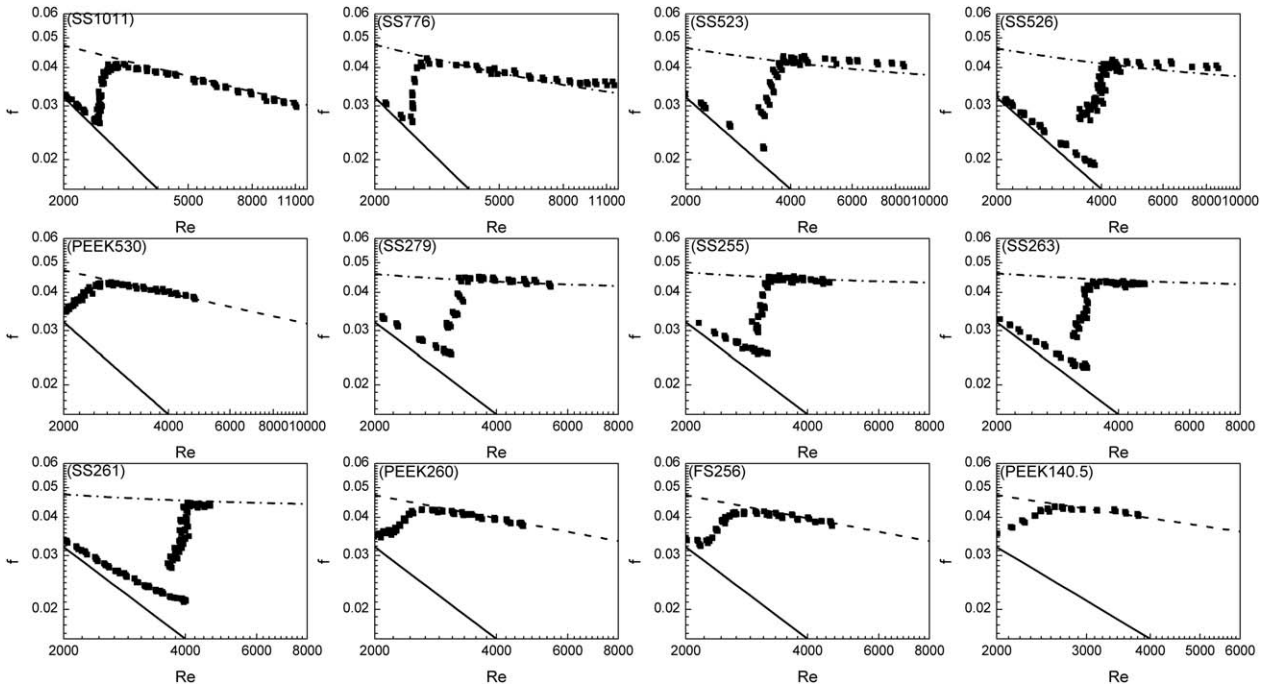

Figure 10. The experimental results of friction factor (*f*) versus Reynolds number (Re) relationship in turbulent flow region of the tested microtubes with diameter $\geq$ 140.5 μm, solid line, Hagen-Poiseuille equation, dash line, Blasius equation, dash dot line, extended Moody equation (Eq. 22).

(SS, FS, and PEEK stand for stainless steel, fused silica, and poly-ether-ether-ketone, respectively, the number stands for the diameter of tested microtube).

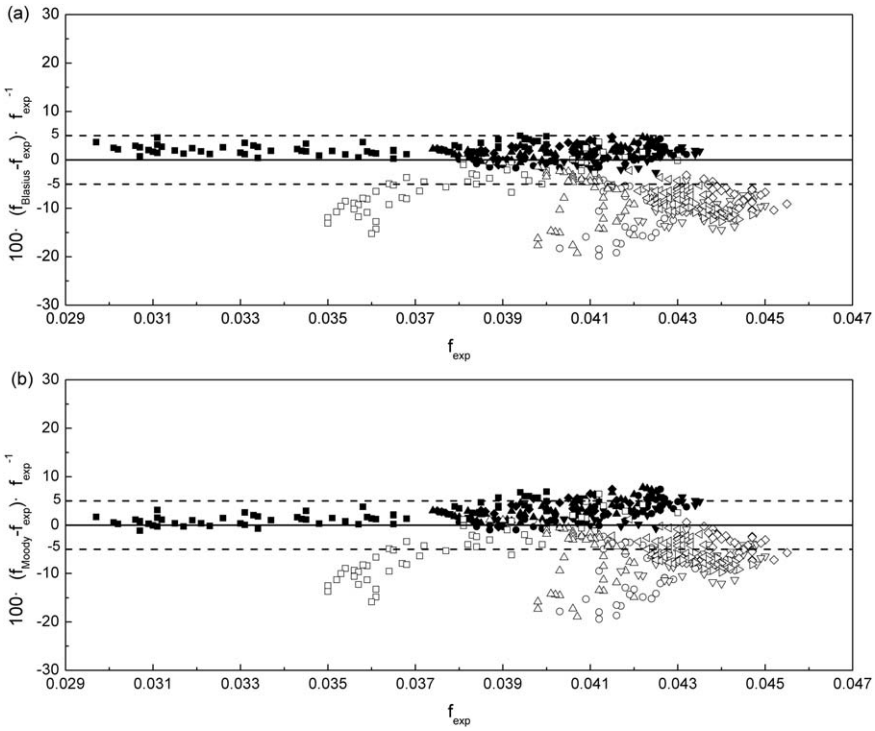

Figure 11. The deviation between the experimental friction factor (f_{exp}) and (a) the calculated friction factor which is obtained through Blasius equation ($f_{Blasius}$), (b) the calculated friction factor which is obtained through Moody equation (f_{Moody}) for all the 538 data points in turbulent flow region, ■, SS1011, •, PEEK530, ▲, PEEK260, ▼, PEEK140.5, ◆, FS256, □, SS776, ○, SS523, △, SS526, ▽, SS279, ◇, SS255, ◁, SS263, ▷, SS261.

(SS, FS, and PEEK stand for stainless steel, fused silica, and poly-ether-ether-ketone, respectively, the number stands for the diameter of tested microtube).

listed in Table 7. It is seen that there is no evident effect of diameter on the range of transitional region as references[43,49] stated. There is also no apparent quantitative relation between roughness and the range of transitional region. However, it is observed that "smooth" microtubes (SS1011, PEEK530, PEEK260, PEEK140.5, and FS256, the roughness (relative roughness) of these five microtubes is in the range from 0.1–0.2 μm (0.02–0.07%)) tend to enter turbulent region earlier than "rough" microtubes (SS776, SS523, SS526, SS279, SS255, SS263, and SS261, the roughness (relative roughness) of these microtubes is in the range from 1.8–3.0 μm (0.23–1.15%)).

The experimental results of f versus Re plots in the transitional flow region (start with Re_c and end with Re_t) of the tested microtubes (diameter $\geq$140.5 μm) are shown in Figure 9. It can be observed from Figure 9 that the friction factor of "rough" microtubes tends to keep decreasing as the increase of Reynolds number for a much longer range than "smooth"

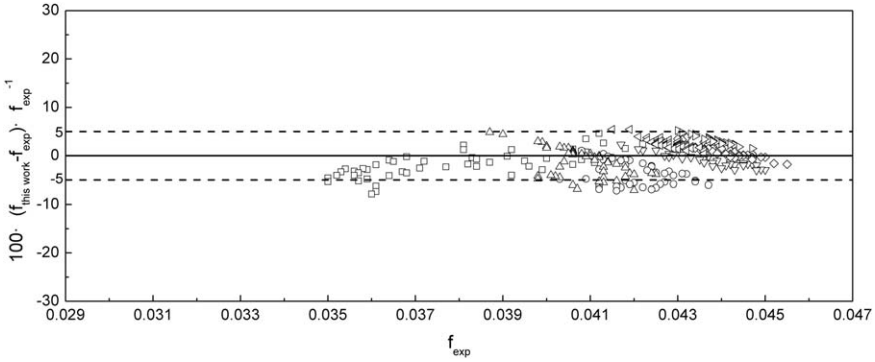

Figure 12. The deviation between the experimental friction factor (f_{exp}) and the calculated friction factor which is obtained through the extended Moody equation (Eq. 22) ($f_{this\ work}$) for the 304 data points in turbulent flow region of rough microtubes, □, SS776, ○, SS523, △, SS526, ▽, SS279, ◇, SS255, ◁, SS263, ▷, SS261.

(SS stands for stainless steel, the number stands for the diameter of tested microtube).

microtubes. Moreover, it is seen that the "smooth" microtubes tend to have a "smooth" transition (the friction factor in the transitional region increases slowly as the Reynolds number increases) and "rough" microtubes tend to have a "rough" transition (the friction factor in the transitional region increases quickly as the Reynolds number increases), which is consistent with the conclusion in literature.[48] For microtubes SS523, SS526, SS279, SS255, SS263, and SS261, a strange phenomenon was observed. As the pressure increases, the Reynolds number increases under normal circumstances. However, at one certain location, the Reynolds number decreases and the friction factor jumps to a much larger value. This phenomenon is only observed in microtubes with roughness (relative roughness) larger than 2.1 μm (0.40%). Further researches are needed to explain the reason.

Turbulent flow region

The liquid flow characteristics in turbulent flow are complex even for conventional sized tubes. Researchers[88–92] are still working on proposing theoretical equation to calculate friction factor in turbulent flow region. People usually use empirical formulas to describe the relationship between friction factor and Reynolds number. The most accurate and accepted formulas are Prandtl's formula (Eq. 17) for smooth pipes, von Karman's formula (Eq. 18) for the fully rough regime, and Colebrook and White's universal formula (Eq. 19).[93]

$$\frac{1}{f^{0.5}} = 2\log\left(\frac{\mathrm{Re}f^{0.5}}{2.51}\right) \tag{17}$$

$$\frac{1}{f^{0.5}} = 2\log\left(\frac{3.7D}{\varepsilon}\right) \tag{18}$$

$$\frac{1}{f^{0.5}} = -2\log\left(\frac{2.51}{\mathrm{Re}f^{0.5}} + \frac{\varepsilon}{3.7D}\right) \tag{19}$$

Equation 19 contains both Eqs. 17 and 18 as limiting cases. However, Eqs. 17 and 19 are implicit equations which need to be solved by iteration and is inconvenient. Many explicit equations have been proposed in the literature. Blasius equation (Eq. 20) and Moody equation (Eq. 21) which are the most simple and classic formulas are chosen to represent the f versus Re relationship of smooth and "rough" (relative roughness in the range of 0–5.00%) conventional sized tubes in this work.

$$f = \frac{0.316}{\mathrm{Re}^{0.25}} \tag{20}$$

$$f = 0.0055\left[1 + \left(2000\frac{\varepsilon}{D} + \frac{1000000}{\mathrm{Re}}\right)^{1/3}\right] \tag{21}$$

The experimental results of f versus Re plots in the turbulent flow region of the tested microtubes (diameter $\geq$140.5 μm) are shown in Figure 10. Figure 11a shows the deviation between the experimental friction factor (f_{exp}) and the calculated friction factor which is obtained through Blasius equation (f_{Blasius}). It is observed that the experimental friction factor in the turbulent region of tested microtubes SS1011, PEEK530, PEEK260, PEEK140.5, and FS256 (234 data points) follows the prediction of Blasius equation perfectly. The AAD is 1.8% for 234 data points with the maximum deviation equals 5.0%. The experimental friction factor in the turbulent region of SS776, SS523, SS526, SS279, SS255, SS263, and SS261 (304 data points) is greater than the prediction of Blasius equation, with an AAD of 8.4% and a maximum deviation of 19.8% for 304 data points. The calculated friction factor which is obtained through Moody equation (f_{Moody}) is slightly larger than f_{Blasius}. As shown in Figure 11b, the AAD is 2.8% for SS1011, PEEK530, PEEK260, PEEK140.5, and FS256 (234 data points) with the maximum deviation equals to 7.8%, and 6.4% for SS776, SS523, SS526, SS279, SS255, SS263, and SS261 (304 data points) with the maximum deviation equals to 19.4%.

It is obvious that Blasius equation can still predict the friction factor for smooth microtubes (SS1011, PEEK530, PEEK260, PEEK140.5, and FS256, the roughness (relative roughness) of these five microtubes is in the range from 0.1–0.2 μm (0.02–0.07%)). However, for rough microtubes (SS776, SS523, SS526, SS279, SS255, SS263, and SS261, the roughness (relative roughness) of these seven microtubes is in the range from 1.8–3.0 μm (0.23–1.15%)), the equations for conventional tubes do not work well. The friction factor is greater than conventional theory and decreases much slower than conventional theory as the increase of Reynolds number. Hence, we believe that it is the enhancement of roughness effect that leads to higher friction factor, the same as also mentioned in literature.[26,41] Some references[26,31,41,45] also have observed higher friction factor, but quantitative study of friction factor (in turbulent flow) in microscale is in a lack. In this work, an extension of Moody equation is proposed to predict the friction factor in microscale. The parameters of the two items in Moody equation, $\varepsilon \cdot D^{-1}$ and Re, are modified with the characteristic parameter α to better predict the friction factor of microtubes in turbulent flow region as follows

$$f = 0.0055\left[1 + \left((1-\alpha)\left(2000(1+70\alpha)\frac{\varepsilon}{D} + \frac{1000000}{\mathrm{Re}}\right)\right)^{1/3}\right] \tag{22}$$

The extended Moody equation (Eq. 22) goes back to Moody equation when D equals 1000 μm (α equals 0). The new obtained Eq. 22 is shown in Figure 10 together with the experimental results of f versus Re relationship in turbulent flow region. The deviation between the experimental friction factor (f_{exp}) and the calculated friction factor which is obtained through the extended Moody equation ($f_{\mathrm{this\ work}}$) is shown in Figure 12. The AAD is 2.4% with a maximum deviation of 7.8%. The calculated friction factor obtained through the extended Moody equation ($f_{\mathrm{this\ work}}$) presents a good agreement with the experimental data (f_{exp}). The results show that the extended Moody equation can predict the friction factor in turbulent flow region (Reynolds number range from 2933–11,644) for microtubes with diameters ranging from 255–776 μm and roughness (relative roughness) in the range of 1.8–3.0 μm (0.23–1.15%) with satisfactory precision. More experiments in microtubes with wide range of diameters and roughnesses need to be conducted to obtain more applicative correlations.

Conclusions

Precise measurements, careful experimental methodology and systematical investigations on liquid flow characteristics in microtubes were performed in this work, using deionized degassed water as working fluid. The friction factor and Reynolds number (2502 data points) have been obtained over a Reynolds number range 29–11,644 for 20 tested

microtubes in the diameter range 44.5–1011 μm, and in the roughness (relative roughness) range of 0.1–5.2 μm (0.02–4.32%).

The conclusions obtained from this work are as follows. (1) In the laminar flow region, the experimental values of Poiseuille number of all the 20 tested microtubes agree well with the conventional theory. There shows no effect of roughness on friction factor (in laminar flow) with roughness (relative roughness) less than 5.2 μm (4.32%). (2) The critical Reynolds number of the tested microtubes with diameters smaller than 1000 μm is in the range of 302–1957, which means that early departure from laminar flow happened for these microtubes. The deviation of critical Reynolds number from conventional theory is found to be caused by the decrease of diameter for microtubes with roughness (relative roughness) less than 10 μm (4.32%), considering the data obtained from this work and references. A parameter α (Eq. 14) was proposed to describe the characteristic of microtube. The characteristic parameter α was used to calculate the critical Reynolds number and a new equation (Eq. 15) was obtained for microscale with an AAD of 1.9%. (3) No apparent quantitative relation between roughness and the range of transitional region was observed as stated in some early references. Nevertheless, smooth microtubes (roughness (relative roughness) in the range 0.1–0.2 μm (0.02–0.07%)) tend to enter turbulent region earlier than rough microtubes (roughness (relative roughness) in the range 1.8–3.0 μm (0.23–1.15%)) in general. Moreover, the friction factor in the transitional region increases slowly as the Reynolds number increases for smooth microtubes, while the friction factor in the transitional region increases quickly as the Reynolds number increases for rough microtubes. (4) In the turbulent flow region, the friction factor values of microtubes with roughness (relative roughness) less than 0.2 μm (0.07%) agree well with the Blasius equation, with an AAD of 1.8%, while the friction factor values of microtubes with roughness (relative roughness) in the range 1.8–3.0 μm (0.23–1.15%) are much greater than the predictions of Blasius equation or Moody equation. An extension of Moody equation (Eq. 22) was proposed with the characteristic parameter α to correlate the data of rough microtubes with satisfactory precision (AAD 2.4%).

Acknowledgment

Financial support from the National Natural Science Foundation of People's Republic of China (project-nos: 21176206 and 21306167) is gratefully acknowledged.

Notation

D = diameter, μm
D_h = hydraulic diameter, μm
$D_{h,cf}$ = constricted hydraulic diameter, μm
D_{in} = inlet diameter, μm
D_{out} = outlet diameter, μm
f = friction factor
fRe = Poiseuille number
L = length of microtube, m
L_{long} = length of the long microtube, m
L_{short} = length of the short microtube, m
M = mass flow rate, kg·s^{-1}
N_p = number of data points
R_a = average roughness, μm
Re = Reynolds number
Re_c = critical Reynolds number
$Re_{c,calc}$ = calculated critical Reynolds number
$Re_{c,cf}$ = critical constricted Reynolds number
Re_t = Reynolds number where turbulent flow begins
Re_0 = critical Reynolds number for $e \cdot D_{h,cf}^{-1} = 0$
R_q = root mean square roughness, μm
T = fluid temperature, °C
α = characteristic parameter of microtube
ΔP = pressure drop, Pa
ΔP_D = pressure losses in hydrodynamic development flow, Pa
ΔP_{FD} = fully developed flow pressure drop, Pa
ΔP_{in} = pressure losses in the inlet, Pa
ΔP_{long} = pressure drop along the long microtube, Pa
ΔP_{out} = pressure losses in the outlet, Pa
ΔP_{short} = pressure drop along the short microtube, Pa
ε = roughness, μm
η = liquid viscosity, Pa·s
ρ = liquid density, kg·m^{-3}
ΣK_L = coefficient to represent additional pressure losses

Literature Cited

1. Zhang J, Wang K, Lin X, Lu Y, Luo G. Intensification of fast exothermic reaction by gas agitation in a microchemical system. *AIChE J*. 2014;60:2724–2730.
2. Fu T, Ma Y, Funfschilling D, Zhu C, Li HZ. Breakup dynamics of slender bubbles in non-newtonian fluids in microfluidic flow-focusing devices. *AIChE J*. 2012;58:3560–3567.
3. Cabeza VS, Kuhn S, Kulkarni AA, Jensen KF. Size-controlled flow synthesis of gold nanoparticles using a segmented flow microfluidic platform. *Langmuir*. 2012;28:7007–7013.
4. Noël T, Kuhn S, Musacchio AJ, Jensen KF, Buchwald SL. Suzuki-Miyaura Cross-Coupling reactions in flow: multistep synthesis enabled by a microfluidic extraction. *Angew Chem*. 2011;123:6065–6068.
5. Zhao C, Miller E, Cooper-White JJ, Middelberg APJ. Effects of fluid-fluid interfacial elasticity on droplet formation in microfluidic devices. *AIChE J*. 2011;57:1669–1677.
6. Wang K, Lu Y, Yang L, Luo G. Microdroplet coalescences at microchannel junctions with different collision angles. *AIChE J*. 2013;59:643–649.
7. Su Y, Chen G, Yuan Q. Influence of hydrodynamics on liquid mixing during Taylor flow in a microchannel. *AIChE J*. 2012;58:1660–1670.
8. Su Y, Zhao Y, Jiao F, Chen G, Yuan Q. The intensification of rapid reactions for multiphase systems in a microchannel reactor by packing microparticles. *AIChE J*. 2011;57:1409–1418.
9. Morini GL. Single-phase convective heat transfer in microchannels: a review of experimental results. *Int J Therm Sci*. 2004;43:631–651.
10. Whitesides GM. The origins and the future of microfluidics. *Nature*. 2006;442:368–373.
11. Hetsroni G, Mosyak A, Pogrebnyak E, Yarin LP. Fluid flow in micro-channels. *Int J Heat Mass Transfer*. 2005;48:1982–1998.
12. Herwig H, Hausner O. Critical view on "new results in micro-fluid mechanics": an example. *Int J Heat Mass Transfer*. 2003;46:935–937.
13. Obot NT. Toward a better understanding of friction and heat/mass transfer in microchannels-a literature review. *Microscale Thermophys Eng*. 2002;6:155–173.
14. Salman BH, Mohammed HA, Munisamy KM, Kherbeet AS. Characteristics of heat transfer and fluid flow in microtube and microchannel using conventional fluids and nanofluids: a review. *Renewable Sustainable Energy Rev*. 2013;28:848–880.
15. Kandlikar SG. History, advances, and challenges in liquid flow and flow boiling heat transfer in microchannels: a critical review. *J Heat Transfer*. 2012;134:34001.
16. Dey R, Das T, Chakraborty S. Frictional and heat transfer characteristics of single-phase microchannel liquid flows. *Heat Transfer Eng*. 2011;33:425–446.
17. Kumar V, Paraschivoiu M, Nigam K. Single-phase fluid flow and mixing in microchannels. *Chem Eng Sci*. 2011;66:1329–1373.
18. Peng XF, Peterson GP, Wang BX. Frictional flow characteristics of water flowing through rectangular microchannels. *Exp Heat Transfer*. 1994;7:249–264.
19. Jiang XN, Zhou ZY, Huang XY, Liu CY. Laminar flow through microchannels used for microscale cooling systems. In: *Proceedings of 1st Electronic Packaging Technology Conference*. Singapore, 1997:119–122.
20. Mala GM, Li DQ. Flow characteristics of water in microtubes. *Int J Heat Fluid Flow*. 1999;20:142–148.

21. Stanley RS, Ameel TA, Barron RF. Two-phase flow in microchannels, North Carolina: U.S. army research office, 1997.
22. Pfund D, Rector D, Shekarriz A, Popescu A, Welty J. Pressure drop measurements in a microchannel. *AIChE J*. 2000;46:1496–1507.
23. Li ZX, Du DX, Guo ZY. Experimental study on flow characteristics of liquid in circular microtubes. *Microscale Thermophys Eng*. 2003; 7:253–265.
24. Ergu OB, Sara ON, Yapici S, Arzutug ME. Pressure drop and point mass transfer in a rectangular microchannel. *Int Commun Heat Mass Transfer*. 2009;36:618–623.
25. Hao PF, He F, Zhu KQ. Flow characteristics in a trapezoidal silicon microchannel. *J Micromech Microeng*. 2005;15:1362–1368.
26. Hrnjak P, Tu X. Single phase pressure drop in microchannels. *Int J Heat Fluid Flow*. 2007;28:2–14.
27. Park HS, Punch J. Friction factor and heat transfer in multiple microchannels with uniform flow distribution. *Int J Heat Mass Transfer*. 2008;51:4535–4543.
28. Schilder B, Man S, Kasagi N, Hardt S, Stephan P. Flow visualization and local measurement of forced convection heat transfer in a microtube. *J Heat Transfer*. 2010;132:31702.
29. Aniskin VM, Adamenko KV, Maslov AA. Experimental determination of the friction factor coefficient in microchannels. *J Appl Mech Tech Phys*. 2011;52:18–23.
30. Barlak S, Yapici S, Sara ON. Experimental investigation of pressure drop and friction factor for water flow in microtubes. *Int J Therm Sci*. 2011;50:361–368.
31. Agostini B, Watel B, Bontemps A, Thonon B. Liquid flow friction factor and heat transfer coefficient in small channels: an experimental investigation. *Exp Therm Fluid Sci*. 2004;28:97–103.
32. Rands C, Webb BW, Maynes D. Characterization of transition to turbulence in microchannels. *Int J Heat Mass Transfer*. 2006;49:2924–2930.
33. Yang CY, Lin TY. Heat transfer characteristics of water flow in microtubes. *Exp Therm Fluid Sci*. 2007;32:432–439.
34. Dutkowski K. Experimental investigations of Poiseuille number laminar flow of water and air in minichannels. *Int J Heat Mass Transfer*. 2008;51:5983–5990.
35. Hao PF, Zhang XW, Yao ZH, He F. Transitional and turbulent flow in a circular microtube. *Exp Therm Fluid Sci*. 2007;32:423–431.
36. Xu B, Ooi KT, Wong NT, Choi WK. Experimental investigation of flow friction for liquid flow in microchannels. *Int Commun Heat Mass Transfer*. 2000;27:1165–1176.
37. Sharp KV, Adrian RJ. Transition from laminar to turbulent flow in liquid filled microtubes. *Exp Fluids*. 2004;36:741–747.
38. Liu Z, Zhang C, Huo Y, Zhao X. Flow and heat transfer in rough micro steel tubes. *Exp Heat Transfer*. 2007;20:289–306.
39. Zhao Y, Liu Z. Experimental studies on flow visualization and heat transfer characteristics in microtubes. In: *Proceedings of 13th International Conference on Heat Transfer*. Sydney, Australia, 2006.
40. Tang GH, Li Z, He YL, Zhao CY, Tao WQ. Experimental observations and lattice Boltzmann method study of the electroviscous effect for liquid flow in microchannels. *J Micromech Microeng*. 2007;17:539–550.
41. Kandlikar SG, Schmitt D, Carrano AL, Taylor JB. Characterization of surface roughness effects on pressure drop in single-phase flow in minichannels. *Phys Fluids*. 2005;17:100606.
42. Brackbill TP, Kandlikar SG. Effects of low uniform relative roughness on single-phase friction factors in microchannels and minichannels. In: *5th International Conference on Nanochannels, Microchannels Minichannels*, 2007:509–518.
43. Ghajar AJ, Tang CC, Cook WL. Experimental investigation of friction factor in the transition region for water flow in minitubes and microtubes. *Heat Transfer Eng*. 2010;31:646–657.
44. Hegab HE, Bari A, Ameel T. Friction and convection studies of R-134a in microchannels within the transition and turbulent flow regimes. *Exp Heat Transfer*. 2002;15:245–259.
45. Celata GP, Cumo M, Guglielmi M, Zummo G. Experimental investigation of hydraulic and single-phase heat transfer in 0.130-mm capillary tube. *Microscale Thermophys Eng*. 2002;6:85–97.
46. Vijayalakshmi K, Anoop KB, Patel HE, Harikrishna PV, Sundararajan T, Das SK. Effects of compressibility and transition to turbulence on flow through microchannels. *Int J Heat Mass Transfer*. 2009;52:2196–2204.
47. Elsnab JR, Maynes D, Klewicki JC, Ameel TA. Mean flow structure in high aspect ratio microchannel flows. *Exp Therm Fluid Sci*. 2010; 34:1077–1088.
48. Bucci A, Celata GP, Cumo M, Serra E, Zummo G. Water single-phase fluid flow and heat transfer in capillary tubes. In: *1st International Conference on Microchannels Minichannels*. Rochester, New York, USA, 2003:319–326.
49. Yang CY, Wu JC, Chien HT, Lu SR. Friction characteristics of water, R-134a, and air in small tubes. *Microscale Thermophys Eng*. 2003;7:335–348.
50. Bhatti MS, Shah RK. Laminar convective heat transfer in ducts. In: Kakaç S, Shah RK, Aung W, editors. *Handbook of Single-Phase Convective Heat Transfer*. New York: Wiley, 1987.
51. Colebrook F. Turbulent flow in pipes with particular reference to the transition region between the smooth and rough pipe laws. *J Inst Civ Eng*. 1939;11:133–156.
52. Blasius H. Das Ähnlichkeitsgesetz bei Reibungsvorgängen in Flüssigkeiten. *VDI Mitt Forschungsarb*. 1913;131 (in German).
53. Miller RW. Flow measurement engineering handbook, 3rd ed. New York: McGraw-Hill, 1996.
54. Churchill SW. Friction factor equations spans all fluid-flow regimes. *Chem Eng*. 1977;45:91–92.
55. Ferguson AD, Bahrami M, Culham JR. Review of experimental procedure for determining liquid flow in microchannels. In: *3rd International Conference on Microchannels Minichannels*, 2005:303–311.
56. Tang GH, Lu YB, Zhang SX, Wang FF, Tao WQ. Experimental investigation of non-Newtonian liquid flow in microchannels. *J Non-Newtonian Fluid Mech*. 2012;173:21–29.
57. Sara ON, Ergu OB, Arzutug ME, Yapici S. Experimental study of laminar forced convective mass transfer and pressure drop in microtubes. *Int J Therm Sci*. 2009;48:1894–1900.
58. Jung JY, Kwak HY. Fluid flow and heat transfer in microchannels with rectangular cross section. *Heat Mass Transfer*. 2008;44:1041–1049.
59. Wu K, Zhao C, Xu G, He C. Investigation of convective heat transfer with liquids in microtubes. *Ind Eng Chem Res*. 2012;51:9386–9395.
60. Hsieh SS, Lin CY, Huang CF, Tsai HH. Liquid flow in a microchannel. *J Micromech Microeng*. 2004;14:436–445.
61. Peng XF, Peterson GP. Convective heat transfer and flow friction for water flow in microchannel structures. *Int J Heat Mass Transfer*. 1996;39:2599–2608.
62. Li Z, He YL, Tang GH, Tao WQ. Experimental and numerical studies of liquid flow and heat transfer in microtubes. *Int J Heat Mass Transfer*. 2007;50:3447–3460.
63. Qu WL, Mala GM, Li DQ. Pressure-driven water flows in trapezoidal silicon microchannels. *Int J Heat Mass Transfer*. 2000;43:353–364.
64. Judy J, Maynes D, Webb BW. Characterization of frictional pressure drop for liquid flows through microchannels. *Int J Heat Mass Transfer*. 2002;45:3477–3489.
65. Parlak N, Gur M, Ari V, Kucuk H, Engin T. Second law analysis of water flow through smooth microtubes under adiabatic conditions. *Exp Therm Fluid Sci*. 2011;35:60–67.
66. Shen S, Xu JL, Zhou JJ, Chen Y. Flow and heat transfer in microchannels with rough wall surface. *Energy Convers Manage*. 2006;47: 1311–1325.
67. Reynaud S, Debray F, Franc JP, Maitre T. Hydrodynamics and heat transfer in two-dimensional minichannels. *Int J Heat Mass Transfer*. 2005;48:3197–3211.
68. Brutin D, Topin F, Tadrist L. Transient method for the liquid laminar flow friction factor in microtubes. *AIChE J*. 2003;49:2759–2767.
69. Celata GP, Cumo M, McPhail S, Zummo G. Characterization of fluid dynamic behaviour and channel wall effects in microtube. *Int J Heat Fluid Flow*. 2006;27:135–143.
70. Celata GP, Morini GL, Marconi V, McPhail SJ, Zummo G. Using viscous heating to determine the friction factor in microchannels—an experimental validation. *Exp Therm Fluid Sci*. 2006;30:725–731.
71. Baviere R, Ayela F, Le Person S, Favre-Marinet M. Experimental characterization of water flow through smooth rectangular microchannels. *Phys Fluids*. 2005;17:98105.
72. Liu D, Garimella SV. Investigation of liquid flow in microchannels. *J Thermophys Heat Transfer*. 2004;18:65–72.
73. Krishnamoorthy C, Ghajar AJ. Single-phase friction factor in microtubes: a critical review of measurement, instrumentation and data reduction techniques from 1991-2006. In: *5th International Conference on Nanochannels, Microchannels Minichannels*. Puebla, Mexico, 2007:813–825.
74. Lin Z. Study on the flow characteristics of ionic liquid aqueous solution in microtube. M.S. Thesis, Zhejiang University, P.R.China, 2013.

75. Zhou Y. Estimation of physical properties of ionic liquids and study on the flow characteristics of ionic liquid ethanol solutions in microtubes. M.S. Thesis, Zhejiang University, P.R.China, 2013.
76. Kandlikar SG, Joshi S, Tian SR. Effect of surface roughness on heat transfer and fluid flow characteristics at low Reynolds numbers in small diameter tubes. *Heat Transfer Eng*. 2003;24:4–16.
77. Tu X, Hrnjak P. Experimental investigation of single-phase flow pressure drop through rectangular microchannels. In: *1st International Conference on Microchannels Minichannels*. Rochester, New York, USA, 2003:257–267.
78. Kohl MJ, Abdel-Khalik SI, Jeter SM, Sadowski DL. An experimental investigation of microchannel flow with internal pressure measurements. *Int J Heat Mass Transfer*. 2005;48:1518–1533.
79. Cui HH, Silber-Li ZH, Zhu SN. Flow characteristics of liquids in microtubes driven by a high pressure. *Phys Fluids*. 2004;16:1803–1810.
80. Brutin D, Tadrist L. Experimental friction factor of a liquid flow in microtubes. *Phys Fluids*. 2003;15:653–661.
81. Zhang XL, Coupland P, Fletcher P, Haswell SJ. Monitoring of liquid flow through microtubes using a micropressure sensor. *Chem Eng Res Des*. 2009;87:19–24.
82. Steinke ME, Kandlikar SG. Single-phase liquid friction factors in microchannels. *Int J Therm Sci*. 2006;45:1073–1083.
83. Streeter VL, Wylie EB. Fluid mechanics, 8th ed. New York: McGraw-Hill, 1985.
84. Moffat RJ. Describing the uncertainties in experimental results. *Exp Therm Fluid Sci*. 1988;1:3–17.
85. Draad AA, Kuiken GDC, Nieuwstadt FTM. Laminar-turbulent transition in pipe flow for Newtonian and non-Newtonian fluids. *J Fluid Mech*. 1998;377:267–312.
86. Eckhardt B, Schneider TM, Hof B, Westerweel J. Turbulence transition in pipe flow. *Annu Rev Fluid Mech*. 2006;39:447–468.
87. Zhou G, Yao S. Effect of surface roughness on laminar liquid flow in micro-channels. *Appl Therm Eng*. 2011;31:228–234.
88. Barenblatt GI. Scaling laws for fully developed turbulent shear flows. Part 1. Basic hypotheses and analysis. *J Fluid Mech*. 1993;248:513–520.
89. Zagarola MV, Smits AJ. Mean-flow scaling of turbulent pipe flow. *J Fluid Mech*. 1998;373:33–79.
90. McKeon BJ, Zagarola MV, Smits AJ. A new friction factor relationship for fully developed pipe flow. *J Fluid Mech*. 2005;538:429–443.
91. Shockling MA, Allen JJ, Smits AJ. Roughness effects in turbulent pipe flow. *J Fluid Mech*. 2006;564:267–285.
92. Churchill SW. New simplified models and formulations for turbulent flow and convection. *AIChE J*. 1997;43:1125–1140.
93. Haaland SE. Simple and explicit formulas for the friction factor in turbulent pipe flow. *J Fluids Eng*. 1983;105:89–90.

Manuscript received July 3, 2014, and revision received Sep. 6, 2014.